Article - Discoveries

Evolutionary trajectories are contingent on mitonuclear interactions

Damien Biot-Pelletier[1,2,3,4]*, Stefano Bettinazzi[5]†, Isabelle Gagnon-Arsenault[1,2,3,4,6], Alexandre K. Dubé[1,2,3,4,6], Camille Bédard[1,2,3,4], Tuc H. M. Nguyen[7]‡, Heather L. Fiumera[7], Sophie Breton[5], Christian R. Landry[1,2,3,4,6]

Affiliations:

[1]Institut de biologie intégrative et des systèmes, Université Laval, Québec QC Canada

[2]Département de biologie, Université Laval, Québec QC Canada

[3]Centre de recherche en données massives (CRDM), Université Laval, Québec QC Canada

[4]PROTEO, le regroupement québécois de recherche sur la fonction, l'ingénierie et les applications des protéines, Université Laval, Québec QC Canada

[5]Département de sciences biologiques, Université de Montréal, Montréal QC Canada

[6]Département de biochimie, microbiologie et bio-informatique, Université Laval, Québec QC Canada

[7]Department of Biological Sciences, Binghamton University, Binghamton NY USA

* Current address: Centre d'expertise en analyses environnementale, Ministère de l'Environnement, et de la Lutte aux changements climatiques, de la Faune et des Parcs, Québec QC Canada

† Current address: Department of Genetics, Evolution and Environment, University College London, London UK

‡ Current address: Department of Biology, New York University, New York NY USA

Corresponding author:

Damien Biot-Pelletier (damien.biot-pelletier@environnement.gouv.qc.ca)

Centre d'expertise en analyse environnementale du Québec

Ministère de l'Environnement et de la Lutte contre les changements climatiques

2700 rue Einstein, Québec QC G1P 3W8

Canada

Abstract

Critical mitochondrial functions, including cellular respiration, rely on frequently interacting components expressed from both the mitochondrial and nuclear genomes. The fitness of eukaryotic organisms depends on a tight collaboration between both genomes. In the face of an elevated rate of evolution in the mitochondrial genome, current models predict that maintenance of mitonuclear compatibility relies on compensatory evolution of the nuclear genome. Mitonuclear interactions would therefore exert an influence on evolutionary trajectories. One prediction from this model is that the same nuclear genomes but evolving with different mitochondrial haplotypes would follow distinct molecular paths towards higher fitness peaks. To test this prediction, we submitted 1344 populations derived from seven mitonuclear genotypes of *Saccharomyces cerevisiae* to more than 300 generations of experimental evolution in conditions that either select for a mitochondrial function, or that do not strictly require respiration for survival. Performing high-throughput phenotyping and whole-genome sequencing on independently evolved individuals isolated from endpoint populations, we identified numerous examples of gene-level evolutionary convergence among populations with the same mitonuclear background. Phenotypic and genotypic data on strains derived from this evolution experiment identify the nuclear genome and the environment as the main determinants of evolutionary divergence, but also show a modulating role for the mitochondrial genome exerted both directly and via interactions with the two other components. We finally recapitulated a subset of prominent loss-of-function alleles in the ancestral backgrounds and confirmed a generalized pattern of mitonuclear-specific and highly epistatic fitness effects. Together, these results demonstrate how mitonuclear interactions can dictate evolutionary divergence of populations with identical starting nuclear genotypes.

Keywords: mitonuclear evolution, mitochondria, evolutionary convergence, experimental evolution

Introduction

According to the endosymbiotic hypothesis, mitochondria derive from an ancestral bacterial symbiont that gradually specialized in its current cellular functions (Dyall et al. 2004; E.S. Fritsch et al. 2014). While most mitochondrial proteins are encoded in the nucleus, the vestigial genome of the organelle retains key genes thought to favor responsiveness to changing conditions (Allen et al. 2003; Lane and Martin 2010; Lane 2011). Gene products encoded in the two genomes are thus required for mitochondrial function. The mitochondrion is now the site of cellular respiration, and as such, plays a central role in energy production (Malina et al. 2018). Other important metabolic processes involve the mitochondrion, including the biosynthesis of heme (Ferreira 1995), iron-sulfur clusters (Read et al. 2021) and steroids (Jordá and Puig 2020). Mitochondria are also involved in nutrient sensing, the regulation of redox homeostasis, and several signaling pathways (Malina et al. 2018).

Components encoded in the nuclear and mitochondrial genomes interact extensively, sometimes encountered together as part of mitochondrial protein complexes (Malina et al. 2018). Cytochrome *c* oxidase (Cooper et al. 1991) and the cytochrome *bc1* complex (Hunte et al. 2003), components of the respiratory electron transport chain, are assembled from proteins encoded by both genomes. In yeast, the mitogenome encodes for mitochondrial ribosomal RNAs and one ribosomal polypeptide, while most protein components are found in the nuclear genome (Desai et al. 2017). In humans, the nucleus-encoded protein LRPPRC is required for cytochrome *c* maturation via interaction with mitochondrial mRNAs, and mutations that alter this function are associated with severe disease (Xu et al. 2012). These examples illustrate the critical importance of mitonuclear interactions, and how their disruption may severely reduce fitness.

Yet, because they are distinct and segregated to separate cell compartments, molecular evolution in the nuclear and mitochondrial genomes is partially uncoupled. Mutation rate tends to be higher in mtDNA (Fritsch et al., 2014; Lynch et al., 2008), especially in organisms with uniparental inheritance and lacking a dedicated mitochondrial mismatch

91 repair system (Mason and Lightowlers 2003; Havird and Sloan 2016). In many organisms,
92 uniparental inheritance also leads to smaller effective population size and the virtual lack
93 of recombination (Lynch et al. 2006; Hagström et al. 2014). More generally, mitochondria
94 evolve in a regulated microenvironment – the cytoplasm with its nuclear supply of
95 mitochondrial proteins – that differs from the extracellular milieu affecting the entire cell.
96 Illustrating this peculiar aspect of mitochondrial evolution is the suppressivity of ρ^-
97 mitogenomes in yeast. In these cells, despite a strongly deleterious effect on organismal
98 fitness, copies of the mitochondrial genome deleted at loci essential for respiration may
99 outcompete healthy copies thanks to their higher replication origin density (de Zamaroczy
100 et al. 1981; Mangin et al. 1983; Bernardi 2005). Furthermore, deletion screens in yeasts
101 have also repeatedly identified signals of frequent essentiality switching among genes
102 involved in mitochondrial functions, both across (Kim et al. 2010) and within species
103 (Caudal et al. 2022; Chen et al. 2022), suggesting enhanced evolvability at these loci. In
104 summary, because of unique characteristics and selection pressures, the rate of evolution
105 tends to be higher in the mitochondrial genome than in the nuclear genome, with a critical
106 influence on genetic divergence, speciation, reproductive strategies, and morphology (Hill
107 2015).
108
109 A model has emerged in which rapid and essentially non-adaptive changes to the
110 mitochondrial genome exert a constant selective pressure on the nuclear genome to
111 accumulate compensatory mutations (Dowling 2014). Rapid changes in mtDNA would
112 drive the nucleus towards increasing divergence, the evolution of Dobzhansky-Muller
113 incompatibilities favoring speciation via post-zygotic reproductive isolation (Freel et al.
114 2015). Such incompatibilities are expected to arise following hybridization between
115 allopatric populations, whose mitonuclear genotypes have evolved independently under
116 different environmental conditions. As extensively described in the copepod *Tigriopus*
117 *californicus*, hybrids may display fitness loss and reproductive incompatibility when
118 initially separated populations come into contact, generating mismatched mitonuclear
119 genotypes (Burton and Barreto 2012; Barreto et al. 2018; Burton 2022). A growing body
120 of evidence accumulates in favor of this model. Early studies showed that species
121 divergence is associated with a loss of mitonuclear compatibility (Niki et al. 1989; Osuský

122 et al. 1997; Dey et al. 2000a; McKenzie and Trounce 2000; Špírek et al. 2000; Yamaoka
123 et al. 2000; Kenyon and Moraes 2002). More recent reports provide examples of
124 reproductive isolation and hybrid fragility associated with mitonuclear incompatibilities
125 (Lee et al. 2008; Chou et al. 2010; Paliwal et al. 2014; Ma et al. 2016; Haddad et al. 2018).
126 The power of mitochondrial markers and genome structures as phylogenetic predictors
127 further supports a driving role for the evolution of mtDNA in divergence and speciation
128 (Robba et al. 2006; Hendrich et al. 2010; Wolters et al. 2015).
129
130 Current understanding about the cell and molecular biology of the mitochondrion owes
131 much to methods and approaches pioneered in the yeast *S. cerevisiae* (Rutter and Hughes
132 2015). As a facultative anaerobe, this yeast can be explicitly selected for respiratory
133 function, via the use of fermentable and non-fermentable carbon sources. This facilitates
134 cytoduction, in which mitochondrial genomes are exchanged between individuals of the
135 same or different species, generating mitonuclear hybrids (Zakharov and Yarovoy 1977;
136 Barrientos et al. 1998). Cytoduction and related methods have been applied to the study of
137 evolutionary questions in mitochondrial biology, for example investigating the
138 compatibility of mitochondrial genomes between closely related species. Coherent with a
139 role for mitochondria in defining the interspecific barrier, these studies showed a rapid
140 decline in the efficiency of oxidative phosphorylation as species divergence increases
141 between the nuclear and mitochondrial parents of mitonuclear hybrids (Barrientos et al.
142 1998; Dey et al. 2000a; Dey et al. 2000b; McKenzie and Trounce 2000; Yamaoka et al.
143 2000; Kenyon and Moraes 2002; Lee et al. 2008; Ma et al. 2016). Cytoduction has also
144 helped identify key genes and molecular functions involved in the mitonuclear
145 incompatibilities that arise between yeast species (Spirek et al. 2015). Collections of yeast
146 mitonuclear hybrids have recently helped explore the genetic space of mitonuclear
147 interactions, revealing the impact of mitonuclear interactions on fitness, and the complex
148 third-order relationships that exist between environmental conditions, the nuclear genome,
149 and the mitochondrial genome (Paliwal et al. 2014; Vijayraghavan et al. 2019; Nguyen et
150 al. 2020).
151

152 Standing models thus predict that mitonuclear interactions must influence the path of
153 evolution. Available evidence from wild individuals and populations supports this model,
154 yet direct experimental testing of this hypothesis in naturally evolving populations is
155 challenging. Experimental evolution in microbes is ideally suited to address this problem,
156 because it can be replicated, enabling the observation of repeatable patterns among
157 identically but independently evolved individuals and populations. Indeed, one of the
158 fundamental questions that underlie much of the experimental evolution literature concerns
159 the predictability of evolution. Given identical genetic and environmental circumstances,
160 will independently evolving populations take the same evolutionary path? Will phenotypes
161 be identical, will the same alleles be selected, or at least will the same genes and functional
162 systems be affected? Repeatable outcomes have been reported in terms of both phenotype
163 and genotype (Wichman et al. 1999; Cooper et al. 2003; Mcdonald et al. 2009; Herron and
164 Doebeli 2013; Lang et al. 2013). Available evidence does not decisively argue for
165 predictability (Bull and Molineux 2008; Łuksza and Lässig 2014), yet the controlled
166 context of experimental evolution seems to lead to evolutionary convergence at the
167 functional complex and gene levels (Tenaillon et al. 2012). Another important advantage
168 of experimental evolution in microbes is the conservation of evolving populations at
169 different steps of the evolutionary process. Evolved individuals can thus be compared
170 experimentally to their ancestors. Mutations selected by evolution can be reconstituted in
171 ancestral backgrounds and assessed for their impact on fitness using marker-assisted
172 competition assays (Breslow et al. 2008; Lang et al. 2013), allowing the precise dissection
173 of the genetic architecture of evolved mutants. Building on these methodological
174 foundations, experimental evolution studies have demonstrated that the path to adaptation
175 is contingent on the genetic makeup of the evolving population and the characteristics of
176 its environment (Blount et al. 2008; Meyer et al. 2012). Therefore, analysis of evolutionary
177 convergence in replicated experimental evolution setups appears as a mean to assess the
178 impact of specific environmental and genetic factors, such as mitonuclear interactions, on
179 evolutionary trajectories and outcomes.
180
181 In this study, we leverage a collection of mitonuclear hybrids from *S. cerevisiae* (Paliwal
182 et al. 2014; Wolters et al. 2018; Nguyen et al. 2020) previously reported to display

183 mitonuclear interactions in a wide array of conditions (Nguyen et al. 2020). To investigate
184 the evolutionary impact of these interactions, we identified example strains from the
185 collection that showed reduced fitness upon mitochondrial replacement. We performed
186 experimental evolution on 1344 replicate populations of the identified strains, varying the
187 intensity of selection on mitochondrial function in an experiment spanning more than three
188 hundred generations. Evolving mitonuclear hybrids provided accelerated mimics of the
189 evolutionary dynamics encountered in organisms with rapidly diverging mitogenomes. The
190 level of replication provided us with a wealth of identically yet independently evolved
191 individuals. We predicted that high-throughput growth assays and whole-genome
192 sequencing on these individuals would allow us to detect patterns of evolution influenced
193 by mitonuclear interactions, at the phenotypic or genotypic levels.
194
195 **Results**
196
197 *Mitonuclear interactions in yeast cybrids*
198 Our founding intent was to study the influence of mitonuclear interactions on the path of
199 evolution. We therefore screened a collection of mitonuclear hybrids of *S. cerevisiae* for
200 evidence of such mitonuclear interactions. This collection contains 225 cybrid strains of
201 yeast generated by cytoduction in four replicates and representing all possible
202 combinations of nuclear and mitochondrial genomes from 15 trains of *S. cerevisiae*
203 (Nguyen et al. 2020). Though widespread mitonuclear interactions were previously found
204 within the collection, we screened it for additional evidence, recording growth rate for all
205 strains as a proxy for fitness in a specific condition – liquid medium with glycerol as the
206 sole carbon source – that requires mitochondrial activity to sustain facultative anaerobic
207 yeast. As observed previously (Nguyen et al., 2020; Paliwal et al., 2014; Wolters et al.,
208 2018), the screen showed the predominant effect of the nuclear genome on fitness but
209 revealed a modulating influence from the mitochondrial genome (**Fig S1**). Some pairs of
210 nuclear and mitochondrial parents displayed a depression in fitness upon cytoduction,
211 potentially indicating mismatched nuclear and mitochondrial genomes. Prominently,
212 mitonuclear hybrids formed between strain DBVPG6044 (D) and strains 273614N (N) and
213 Y12 (Y) were submitted to further scrutiny to formally test the phenotypic influence of the

214 nuclear and mitonuclear genomes and their interactions (**Fig 1, S2**). Following a two-letter
215 nomenclature, indicating the nuclear background first and the mitochondrial background
216 second, genotypes of interest were: NN, ND, DN, DD, DY, YD, and YY (**Fig 1**A). These
217 genotypes can be regarded as two sets of mitonuclear swaps: the N<->D set consisting of
218 genotypes NN, ND, DN, DD; and a D<->Y swap consisting of DD, DY, YD, YY. We
219 estimated fitness of the strains by recording their growth rate and carrying capacity in two
220 environments: fermentable (FF) and non-fermentable (NF) media, containing glucose and
221 glycerol as the sole carbon source, respectively. For the two sets of mitonuclear swaps, we
222 drew interaction plots and performed two-way ANOVAs to test the influence of both
223 genomes and their interactions on fitness (**Fig 1**B**, S2**). Consistent with previous
224 observations, the nuclear genome appeared as the main determinant of fitness, significantly
225 affecting growth in all conditions and for all growth parameters, with the mitochondrial
226 background playing but an occasional role. Notably, we noted that growth was dependent
227 on statistically significant mitonuclear interactions in both sets. We also assayed the
228 activity of a panel of enzymes associated with the mitochondrion in whole cell lysates of
229 the same strains grown in non-fermentable medium (**Fig S3**). Independent effects of
230 nuclear and mitochondrial genomes and interacting mitonuclear effects varied depending
231 on the enzyme assays and strain set. Significant effects for mitonuclear interactions were
232 detected for malate dehydrogenase (N<->D) (**Fig 1**C), citrate synthase (N<->D), and
233 ATPase (D<->Y) (**Fig S3**). We thus accumulated a body of evidence demonstrating
234 mitonuclear interactions by showing that interrupting coevolved mitonuclear genotypes
235 alters fitness in strains N, D, Y and their cybrid derivatives. This enabled further studies on
236 the evolutionary influence of mitonuclear interactions in yeast.
237
238 *Yeast mitonuclear hybrids submitted to experimental evolution undergo fitness changes*
239 *influenced by mitonuclear interactions*
240 We evolved 96 populations for each of the seven mitonuclear backgrounds derived from
241 strains N, D and Y. This experiment was performed in conditions that require or do not
242 require mitochondrial respiration using non-fermentable and fermentable sugars,
243 respectively. We cultured 1344 independently evolving populations by daily serial passage
244 for 58 days, amounting to approximately 300 generations (**Fig 2**A). Frozen stocks were

245 prepared at the beginning and end of the experiment, as well as every seventh passage. A
246 subset of 230 populations went extinct or were terminated because of bacterial
247 contamination, while 1114 populations survived to the end. A single individual was
248 isolated by streaking for single colonies from stocks of each of the surviving populations.
249
250 We next measured the extent of adaptation in evolved individuals by recording growth on
251 both fermentable and non-fermentable media, in an automated and highly replicated
252 manner (**Fig S4**). As expected, the evolved isolates generally displayed median fitness
253 above ancestral values, but the magnitude of the gains was dependent on the fitness of the
254 founding strains (**Fig 2**B). Best illustrating this trend are strains carrying the D nuclear
255 genome for which comparingly low initial fitness in fermentable media represented
256 potential for large gains (**Fig 2**B). In comparison, mean fitness gains in fermentable
257 medium are modest if not null in backgrounds carrying the Y and N nuclei. Interestingly,
258 a similar endpoint fitness, close to the value of the fittest ancestors (NN, YY) is reached
259 across backgrounds in fermentable medium suggesting that evolved clones are, on average,
260 approaching fitness optimum in this environment. Evolution in non-fermentable medium
261 also generally led to higher median fitness. Here also, the N nuclear genome is associated
262 with the lowest median fitness among evolved individuals. For example, in fermentable
263 medium, NN and ND individuals evolved in non-fermentable conditions generally appear
264 less fit than their ancestors. This further indicates that, in fermentable medium, these strains
265 are close to fitness optimum, where most mutations are expected to be deleterious,
266 including those that are adaptive in other environments. Of note, in non-fermentable
267 medium, the fittest of the ancestral backgrounds (YY) also displays one of the largest
268 median gains in fitness, suggesting individuals evolved in this environment are still largely
269 far from fitness optimum.
270
271 All evolved individuals were assayed for growth in fermentable and non-fermentable
272 media. Gains achieved through evolution in one carbon source often translated into gains
273 in the other. Indeed, in most mitonuclear backgrounds, individuals evolved in fermentable
274 and non-fermentable medium display similar fitness in both carbon sources (**Fig S4**).
275 Strikingly, in non-fermentable conditions, strains evolved in this medium are frequently

276 matched or outperformed by those evolved in fermentable medium (**Fig S4**BD), as they
277 likely spent a portion of each evolution cycle respiring in the stationary phase. Similarly,
278 in fermentable medium, while non-fermentable-evolved individuals tend be less fit than
279 their fermentable-evolved counterparts, they still demonstrate significant fitness gains over
280 ancestral levels (**Fig S4**AC). These observations suggest that much of the gain in fitness is
281 related to aspects common to both environments, either in terms of media composition or
282 culture conditions.
283
284 We used the fitness of evolved individuals to test the effect of mitonuclear interactions on
285 evolutionary outcomes. We drew interaction plots and performed two-way ANOVAs,
286 revealing patterns of relative fitness that bore both resemblances and differences with those
287 of ancestral strains (**Fig 2**C, **S5**). Nuclear effects on fitness are most frequent in both
288 ancestral and evolved strains. However, evidence for the influence of the mitochondrial
289 background and mitonuclear interactions is more frequent in fitness data of the evolved
290 strains. These results show an influence for mitonuclear interactions on the outcomes of
291 experimental evolution at the phenotype level.
292
293 *Sequencing of evolved genomes reveals patterns of evolutionary convergence.*
294 To probe the molecular mechanisms involved in the adaptation of evolved isolates, we
295 sequenced each of their genomes, along with that of their ancestors, aligning to published
296 sequences of ancestral nuclear and mitochondrial backgrounds. Our partially redundant
297 dataset comprised 1505 non-empty sequencing libraries and provided genomic data for
298 1114 evolved isolates and 28 ancestral strains. With a 31x median depth of coverage, most
299 libraries were suitable for the confident calling of mutations, from the whole-chromosome
300 to single-nucleotide scales (**Data S1**). We first examined chromosome-scale changes,
301 beginning with the mitochondrial genome. In contrast with published methods that rely on
302 median depth at stably covered loci *COX1* or *COX3* (Puddu et al., 2019), and
303 acknowledging the complex and highly branched topology of *S. cerevisiae* mtDNA
304 (Bendich 1996; Bendich 2007), we abstained from claims about mitogenome copy number,
305 and used the fraction of sequence bases mapped to coding regions of the mitochondrial
306 genome to probe general changes to mtDNA, including structure, copy number and others,

307 incurred via experimental evolution and cybridization (**Fig 3**A). Because of disparities in
308 the sequence, structure and quality of the reference mitochondrial genomes, we restricted
309 comparisons to strains that share the same mitochondrial background. We observed
310 changes in mtDNA among the ancestral mitonuclear hybrids, echoing enzyme assays (**Fig**
311 **S3**) hinting to changes in mitochondrial metabolism upon cytoduction. We also observed
312 a trend towards a decrease in the fraction of coding mtDNA in evolved isolates. This
313 change is likely not the result of widespread petite genotypes, since most isolates display
314 fitness in non-fermentable media that is equal or superior to their non-evolved ancestors
315 (**Fig S4**BD). Similarly, extent of the contraction in mtDNA fraction is dependent on both
316 mitonuclear background and evolution conditions. Because environmental demands on
317 respiratory metabolism affect mtDNA copy numbers, our observations about mtDNA
318 fraction are chiefly relevant to the fermentable conditions in which we propagated the yeast
319 used for gDNA extraction (Galeota-Sprung et al., 2022).
320
321 We detected copy number increases for several chromosomes, prominently including
322 chromosomes XII, IV and IX (**Fig 3**B, **Fig S6**). We detected aneuploidies at chromosome
323 XII in 50 independently evolved strains: these changes were significantly enriched in
324 presence of the N nuclear genome and the matching mitochondrial genome. We observed
325 a similar pattern for aneuploidies of chromosome IV. We most often found extra copies of
326 chromosome IX in mitonuclear hybrid derivatives of strain D (**Fig 3**B). Along with changes
327 in mtDNA, these repeated large-scale genomic changes suggested a pattern of convergent
328 evolution influenced by the identity and interaction of nuclear and mitochondrial genomes.
329
330 We next identified smaller scale genetic changes. Following stringent bioinformatics
331 pipelines, we called 272 copy number variants (CNVs), ranging in size from 184 bp to
332 1091 bp, and 3710 single nucleotide variants (SNVs) (**Data S3**). Neither CNVs nor SNVs
333 were distributed randomly among mitonuclear backgrounds and carbon sources (chi^2 test
334 p-values < 0.05). This fact may appear most obvious observing that only nine CNV calls
335 were made in nuclear derivatives of strain D. In stark contrast, ND derivatives evolved in
336 fermentable medium and YD derivatives evolved in non-fermentable medium accumulated
337 92 and 86 CNVs, respectively (**Fig 3**B). One may note that both backgrounds derive from

338 mitochondrial swaps. In the same way, SNVs are unevenly distributed, yet the large
339 number of calls ensures that more than a hundred mutations were detected per mitonuclear
340 background in each carbon source. Together, these small-scale changes provided further
341 hints that both mitonuclear interactions and the environment inflected adaptive trajectories
342 in our mitonuclear hybrids.
343
344 *Dissimilar mutational profiles provide evidence for mitonuclear specific evolutionary*
345 *trajectories*
346
347 From the distribution of aneuploidies and CNVs we hypothesized that each mitonuclear
348 background and each carbon source could be associated with at least partially distinct sets
349 of mutations. We tested this hypothesis by calculating Bray-Curtis dissimilarity between
350 the sets of mutations accumulated by each background in each environment (**Fig S7**).
351 While variable, mean dissimilarity between the mutational profiles of all pairs of
352 evolutionary conditions is high at 0.93. To better grasp the influence of carbon sources and
353 nuclear and mitochondrial backgrounds on mutational profiles, we used the dissimilarity
354 matrix as input for non-parametric multi-dimensional scaling (NMDS, **Fig 4**A). Strikingly,
355 this analysis reveals a broad pattern in which backgrounds evolved in the same
356 environment cluster together along a single axis. A shared nuclear background is also
357 associated with smaller distances and a tendency to cluster together. This analysis also
358 suggests that the mitochondrial background more modestly influences mutational
359 divergence. Visual examination of the dissimilarity matrix (**Fig S7**) also suggested that a
360 shared nuclear background or evolution in the same environment could be associated with
361 reduced dissimilarity in mutational profile. We formally tested these intuitions by
362 partitioning the dissimilarity matrix according to match or mismatch with respect to
363 environment, nuclear background, and mitochondrial background (**Fig 4**B). We performed
364 a three-way ANOVA on the data partitioned in this way, revealing a significant effect on
365 dissimilarity for all three matches and their interactions. Lowest dissimilarities are
366 associated with pairs that display a single mismatch, either at the mitochondrial or
367 environmental levels, whereas mismatched nuclei suffice to maximize dissimilarity.
368 Highest dissimilarity is observed when both the environment and the nucleus differ,

369 regardless of the mitochondrion. Together, these results confirm NMDS outcomes by
370 ascribing a major role in mutational divergence to the nuclear background and identifying
371 the environment as more impactful than the mitochondrial background. Critically, all three
372 aspects impact evolutionary divergence and interact to yield dissimilar mutational profiles.
373
374 We next asked if patterns of specificity were observed at the gene level and examined
375 annotations associated with CNV and SNV calls (**Data S4**). Like aneuploidies, gene-level
376 annotation indicated evolutionary convergence at several loci. Indeed, hundreds of genes
377 are associated with more than one mutation among evolved clones, and 43 display ten or
378 more. Along with aneuploidy at chromosome XII, nuclear genes *RSN1*, *HPF1*, *MNN4*,
379 *AMN1* and mitochondrial gene *COX1* are the annotations associated with the strongest
380 signals of evolutionary convergence, with tens to more than a hundred calls per locus
381 mapping to these areas of the genome. Examining mutation counts associated with these
382 loci in each mitonuclear background and carbon source (e.g. **Fig S8**), we detected several
383 examples of potential specificity.
384
385 Our survey of genetic changes in evolved individuals, at all scales examined, thus provided
386 evidence for evolutionary convergence within a given mitonuclear background, and
387 strongly suggested that adaptive changes followed a pattern of specificity to both
388 mitonuclear background and environmental conditions. To test this hypothesis, for each
389 annotation, we performed chi^2-tests of independence on contingency tables partitioning all
390 mutations according to their association with the annotation, and according to either
391 mitonuclear background or carbon source. We also computed mutual information from the
392 same contingency tables. Both a significant p-value from this test and significantly above
393 average mutual information were required to identify specific annotations (**Fig 4**C). Similar
394 computations were performed, partitioning mutation counts according to nuclear and
395 mitochondrial backgrounds alone, or conjunctions of background with carbon source (**Fig**
396 **S9**). These analyses revealed areas of the yeast genome biased towards de novo mutation
397 in a mitonuclear background- and carbon source-specific manner. For example, out of 50
398 aneuploidies detected at chromosome XII, 38 were found in background NN, and they
399 appear to have been selected almost exclusively in non-fermentable medium. Similarly,

400 94% of the 88 CNVs at gene *HPF1* were selected in background ND evolving in
401 fermentable medium (**Fig S8**). From this data and our earlier analysis of mutational
402 dissimilarity, we concluded that interactions of the environment with both nuclear and
403 mitochondrial backgrounds inflected evolutionary trajectories at the molecular level.
404
405 *Reconstituting loss-of-function mutations in ancestral backgrounds leads to mitonuclear*
406 *background-specific fitness effects*
407 Collected evidence suggested each mitonuclear background accumulated a distinct set of
408 mutations during adaptive evolution. Therefore, we hypothesized that the phenotypic
409 effects of individual mutations selected during the experiment were epistatic with the
410 mitonuclear background. We tested the statistical association between mutant annotations
411 and available phenotype measurements and found several candidate causal loci (**Fig S10**).
412 From this list of loci, patterns of convergent evolution and both mitonuclear and carbon
413 source specificity, we identified a core set of annotations potentially involved in adaptation
414 or otherwise implicated in the evolution of our mitonuclear hybrids. Mapping of mutations
415 on these annotated features and prediction of their mutational effects revealed widespread
416 stop codons alongside missense mutations at conserved positions (e.g., **Fig S11**). We
417 therefore hypothesized that loss-of-function at these and other loci was a widespread
418 adaptive mechanism selected by our experiment, as observed for other experimental
419 populations evolved in constant environments (Kvitek and Sherlock 2013).
420
421 To mimic the effect of loss-of-function alleles, we generated a replicated set of knockouts
422 in fluorescent derivatives of each of the seven ancestral backgrounds at eight loci identified
423 in our dataset. Loci were chosen based on frequency of mutation, statistical association
424 with changes in phenotype, technical feasibility, gene essentiality, and both mitonuclear
425 and carbon source specificity. We competed the knockouts against their wild type
426 counterparts in the conditions of the evolution experiment. From these competitions, we
427 estimated the fitness effect of loss-of-function at these loci in all mitonuclear backgrounds
428 and both fermentable and non-fermentable media (**Fig 5**). Loss-of-function at these loci led
429 in most cases to significant gains in fitness, validating their roles in adaptive evolution. The
430 magnitude of the changes in fitness associated with each knock-out differed significantly

431 between mitonuclear backgrounds and was influenced by nuclear and mitochondrial
432 backgrounds as well as mitonuclear interactions (two-way ANOVA p-value < 0.05, **Fig**
433 **S12**). Some loci even showed opposite effects between different mitonuclear backgrounds,
434 further underlining the strongly epistatic nature of their impact on fitness. This result
435 provided additional support for a decisive role of mitonuclear interactions in shaping and
436 inflecting the path of adaptive evolution.
437
438 Competition assays provided additional support for evolution contingent on mitonuclear
439 interactions. Yet, for most tested loci, differential fitness effect patterns did not match
440 predictions derived from our analysis of evolutionary convergence (**Fig 5**, **Fig S13**).
441 Contrary to expectation, apart from *RIM20* knockouts growing in fermentable medium,
442 rank correlation was poor between estimated fitness effects and mutation frequency in
443 evolved mutants (Spearman correlation p-value on the slope > 0.05). In other words,
444 frequent mutation at a locus does not reliably predict strong gains in fitness in knockouts
445 of that locus. In contrast, in fermentable medium, predictions of locus preference based on
446 mutation frequency matched fitness effect-based predictions of preference, for half of our
447 mitonuclear backgrounds (**Fig 5, Fig S13**).
448
449 We explored possible explanations for the partial disconnect between convergence- and
450 fitness effect-based predictions. The experiment was based on the simplifying assumption
451 that complete loss-of-function is the primary and sole mechanism underlying the fitness
452 effect of mutation at all examined loci. Different or concurring mechanisms are likely
453 involved and may explain some of the discrepancy between fitness data and our analysis
454 of evolutionary convergence. Such mechanisms may include protein truncation, loss of
455 regulatory interactions, and partial reductions in activity, to name but a few. Yet, beside
456 the raw fitness effect of mutations in the ancestral strains, other mechanisms not related to
457 mitonuclear interactions may account for the observed patterns of mitonuclear and carbon
458 source specificity. Fitness of the ancestral strains (**Fig 1**B**, Fig S2**) differs markedly
459 between mitochondrial backgrounds. If the fittest backgrounds are indeed approaching
460 fitness optimum, as hypothesized above, and given patterns of diminishing returns epistasis
461 common in experimental evolution (Chou et al. 2011; Wiser et al. 2013; Couce and

462 Tenaillon 2015), the magnitude of fitness gains accessible to different mitonuclear pairs
463 likely differed, constraining evolutionary paths to adaptation. Considering that initial
464 fitness itself is influenced by mitonuclear interactions, this effect may prove difficult to
465 deconvolute from other similarly influenced mechanisms. However, we did identify loci
466 uniquely or preferentially mutated in mitonuclear backgrounds that otherwise display
467 comparable initial fitness to closely related backgrounds (**Fig S8**). We also counted the
468 number of non-synonymous mutation calls in evolved individuals. We found that the
469 median number of mutations detected per evolved individual is two (**Data S3**). Hence, in
470 evolved individuals, loss-of-function alleles normally interact with other mutant loci,
471 contrary to our simplified experiment, performed in the ancestral backgrounds. This aspect
472 appears critical when considering mutational order: selection for mutation at any given
473 locus is contingent on the identity of mutations most likely to fix earlier during evolution
474 (Weinreich et al. 2006). This itself may be influenced by mitonuclear interactions and
475 illustrates the difficulty of predicting patterns of mutational specificity and evolutionary
476 convergence based solely on fitness effects measured in the ancestral strains.
477
478 We also found that the nucleotide-level mutational profile observed in backgrounds NN
479 and YY differed slightly but significantly from that of all other strains (**Fig S14**). This
480 mutational bias would support the hypothesis that patterns of background-dependent
481 evolutionary convergence may, at least in part, be dictated by differential access to
482 beneficial mutations rather than mitonuclear interactions. Yet, because the nuclear genome,
483 by virtue of its much larger size, chiefly determines mutational bias, this hypothesis does
484 not account for differences in mutational specificity observed between backgrounds that
485 carry the same nuclear genome (as illustrated in **Fig S8**). Moreover, fitness effects inferred
486 from association tests in evolved mutants also correlated poorly with both convergent
487 evolution signals and competition data (**Fig S13**). Together, these results indicate that
488 different mitonuclear backgrounds may have access to different mutational spectra, in
489 presence of multiple and complex epistatic networks. Mitonuclear interactions are a critical
490 component of these epistatic networks and appear to exert a decisive impact on the path of
491 evolutionary adaptation in *S. cerevisiae*.
492

493 **Discussion**

494

495 The current model of mitonuclear evolution proposes that the mitochondrial genome,
496 through interactions with nucleus-encoded genetic material, exerts an influence on
497 evolutionary divergence of populations and eventually on the process of speciation. An
498 elevated rate of evolution observed in the mitogenome can exert a pressure for
499 compensatory evolution of the nuclear genome, leading to negative interactions between
500 mitonuclear pairs that have evolved independently (Dowling 2014). Evidence of
501 mitonuclear incompatibility between both closely related species (Niki et al. 1989; Osuský
502 et al. 1997; Dey et al. 2000a; McKenzie and Trounce 2000; Špírek et al. 2000; Yamaoka
503 et al. 2000; Kenyon and Moraes 2002; Lee et al. 2008; Chou et al. 2010; Ma et al. 2016)
504 and geographically isolated populations of the same species (Paliwal et al. 2014; Wolters
505 et al. 2015; Barreto et al. 2018; Wolters et al. 2018; Nguyen et al. 2020) corroborates this
506 model. Yet, direct experimental evidence demonstrating the impact of mitonuclear
507 interactions on evolutionary trajectories and outcomes was still lacking. We designed an
508 experimental evolution study aimed at filling this gap. We mimicked the potential pressure
509 exerted by the mitochondrial genome on the nuclear genome by swapping mitochondrial
510 genotypes among yeast strains. We propagated these strains in a highly replicated manner
511 for several hundred generations in conditions that either explicitly select for a
512 mitochondrial function or relax the selective pressure exerted on this function. If the
513 mitochondrial genome exerts a pressure on the nuclear genome, independent populations
514 of the same nuclear genotypes but with distinct mitochondrial haplotypes should converge
515 on different adaptive mutations.

516

517 *Mitonuclear interactions and their impact on evolutionary trajectories*

518 The outcomes of our evolution experiment and the analyses herein support our prediction
519 that specific mitonuclear interactions led to distinct evolutionary trajectories. Our
520 phenotypic data shows the influence exerted on fitness of mitonuclear interactions in both
521 ancestral and evolved individuals. Such effects depended on the conditions in which they
522 were tested, the evolution regimen, and fitness proxies retained for analysis. Fitness in the
523 evolved individuals that we isolated is on average comparable albeit not identical among

524 the mitonuclear backgrounds under study. Genomic scrutiny in those individuals provides
525 additional evidence for the impact of mitonuclear interactions on evolutionary outcomes.
526 Thanks to our highly replicated dataset, we were able to detect signals of evolutionary
527 convergence within starting genotypes at the whole-chromosome and gene levels, as
528 observed in previous evolution experiments (Tenaillon et al. 2012). This allowed us to
529 identify features of the yeast genome specifically or preferentially targeted by selection in
530 a mitonuclear background-specific manner. This included changes that were specific to one
531 single mitonuclear background, to the exclusion of closely related ones. We similarly
532 detected environment-specific patterns of selection. Furthermore, recapitulating loss-of-
533 function alleles at convergent loci in the ancestral strains of our experiment, we
534 demonstrated that their effect on fitness, while generally favourable, varied markedly as a
535 function of mitonuclear background and carbon source. Taken together, this evidence
536 therefore upholds standing models of mitonuclear evolution, whereas specific interactions
537 between the nuclear and mitochondrial genomes lead to divergent evolutionary trajectories.
538
539 Screening our collection of mitonuclear hybrids, we observed that the starting nuclear
540 genome exerted a larger impact on fitness than did the mitochondrial genome. Highly
541 replicated assessment of fitness in the ancestral strains confirmed this observation but
542 indicated a modulating influence for the mitochondrial genome and mitonuclear
543 interactions. Further supporting this view, we found evidence that the disruption of co-
544 evolved mitonuclear pairs via cytoduction can impact the activity of mitochondrial
545 enzymes and is associated with changes in mtDNA content. These founding contingencies
546 in the experimental evolution represent, on their own, strong predictors of the divergent
547 evolutionary trajectories predicted from different mitonuclear backgrounds. Indeed, the
548 contingent evolutionary history of an organism creates a unique ensemble of constraints on
549 the set of alleles likely favored by selection. In other words, it potentiates specific
550 evolutionary pathways, and examples of this are reported in the experimental evolution
551 literature (Blount et al. 2008).
552
553 Evolved individuals displayed greater phenotypic uniformity than their unevolved
554 ancestors. Less adapted mitonuclear backgrounds readily caught up to fitter ones. This is

555 coherent with the rapid and reproducible gains in fitness generally observed in the early
556 stages of experimental evolution (Wiser et al. 2013) and with patterns of diminishing
557 returns epistasis expected in fitter individuals (Chou et al. 2011; Couce and Tenaillon
558 2015). Evolved individuals display phenotypic uniformity in the environment in which
559 they evolved, but also in conditions to which they were not explicitly adapted. This could
560 be a sign of positive pleiotropy, meaning that many of the mutations selected in one
561 environment tend to be adaptive in the other. More prosaically, we note that the two
562 environments differ solely by the identity of the available carbon source. Hence, we posit
563 that both environments are more alike than different, and alleles selected in either will tend
564 to be adaptive in both by virtue of the same mechanisms. Despite this, we did observe
565 several environment-specific mutant annotations. We also observed slightly lower fitness
566 in fermentable medium for individuals evolved in non-fermentable medium. Therefore,
567 environment-specific adaptive strategies still arose, which may steer the path of evolution
568 towards more strongly distinct pathways over a longer evolutionary period.
569
570 Mitonuclear cooperation posits a complex network of genetic and physical interactions.
571 Compatible with this framework, patterns of mitonuclear-specific evolutionary
572 convergence and mitonuclear interactions presented in this study suggest selection affected
573 by high-order epistasis. Recapitulating some of the selected mutations as loss-of-function
574 alleles further argued for that view, as their effect in the ancestral backgrounds was
575 dependent on the mitonuclear background. Furthermore, the locus preferences we could
576 infer from the fitness of these reconstituted mutants did not match predictions from patterns
577 of evolutionary convergence. Since we know that each evolved individual carries more
578 than one mutation, we can reasonably posit that the effect of mutation at any locus in our
579 mutants, and the probability for their selection during evolution, is affected by other
580 mutations found in the same cells, especially those that arose earlier. The factor that unifies
581 all these considerations is the founding difference in mitonuclear background.
582
583 *Limitations of the study*
584 Our evolution experiment lasted approximately 300 generations. While published
585 experimental evolution studies of a few hundred generations are common, this remains

586 short on the evolutionary time scale. For comparison, this would correspond to roughly
587 7500 years of human evolution. While most studies cannot realistically last for tens of
588 thousands of generations, a few thousand generations are commonplace (Lenski 2017). The
589 typical workaround for short-term experimental evolution is increased replication
590 (Mcdonald 2019). With more than 1300 starting populations, our experiment certainly
591 meets the high replication standard, yet studies with similar levels of replication have
592 reported lengths of up to a thousand generations (Lang et al. 2011; Lang et al. 2013).
593 Despite this limitation, we were able to identify numerous and clear patterns of
594 evolutionary convergence within genotypes. In addition, we could assign both mitonuclear
595 and carbon source specificity to many mutant loci. Furthermore, it is uncertain that
596 prolonged evolution would have increased the statistical power of our study. While it may
597 have exacerbated patterns of specificity at some loci, over long periods, the accumulation
598 of fixation events coupled to clonal interference and negative epistasis could have reduced
599 the diversity of detectable patterns. However, it could also have enabled the detection of
600 patterns that could only emerge after the fixation of earlier mutations. In short, by affording
601 time for divergence, a longer evolution may have helped observe more sharply defined
602 evolutionary trajectories for each mitonuclear background.
603
604 By evolving yeast in two environments that differed solely by the identity of the available
605 carbon source, we hoped to test for the effect of explicitly selecting for a mitochondrial
606 function, while minimizing confounding factors. In retrospect, comparing outcomes of
607 evolution in two highly similar environments may have led to excessively similar
608 outcomes, especially at the phenotypic level. Variation of an additional factor, such as
609 nitrogen source, temperature, or even carbon source concentration, may have helped
610 further differentiate populations evolving in distinct conditions, and better identify effects
611 specific to mitochondrial function. Nevertheless, our experimental setup proved sufficient
612 to identify carbon source-specific mutational patterns and compare patterns of divergence
613 associated with different selective pressures.
614
615 The seven mitonuclear backgrounds that we submitted to experimental evolution were
616 derived from just three original strains. We screened our collection of cytoductants for

617 mitonuclear mismatches with readily detectable phenotypic differences, maximizing our
618 chances of observing bona fide examples of mitonuclear interactions. This may have
619 unduly restricted the breadth of observable patterns of mitonuclear interaction and
620 evolution, biasing our results towards specific evolutionary outcomes. An alternative
621 would have been to propagate a much wider diversity of mitonuclear backgrounds,
622 potentially evolving our entire collection. This agnostic approach would have limited
623 potential artefactual biases induced by the experimental design, at the expense of per
624 background replication.
625
626 Most of the evidence presented in this study relies directly or indirectly on the results of
627 sequencing. We did phenotype each of our evolved isolates. We also attempted
628 recapitulation of some of the loss-of-function alleles identified by sequencing, generating
629 corresponding knockouts in ancestral backgrounds. Yet, these experiments either
630 imperfectly mimicked the conditions of evolution, were limited in scope or relied on
631 simplifying assumptions. Indeed, systematic assessment of growth kinetics in evolved
632 isolates was performed on solid medium for ease of replication and automation, whereas
633 evolution was performed in liquid to accelerate evolution. Thus, phenotypic insight from
634 growth on solid may not accurately reflect growth in the conditions of evolution. In
635 contrast, high-sensitivity competition assays on recapitulated loss-of-function alleles
636 assessed fitness effects in the exact conditions used for evolution. Yet, those assays
637 concerned but a limited number of loci. For technical reasons, mutations to the
638 mitochondrial genomes and aneuploidies had to be excluded from these tests. More
639 generally, our restricted choice of loci may not reflect most mutations, biasing our view of
640 fitness effects. Potentially more impactful is our simplifying assumption that mutations at
641 the chosen loci were pure loss-of-function alleles, which we chose to recapitulate using
642 whole gene knockouts. Careful reconstitution of the exact mutations identified by
643 sequencing, while less scalable, may have provided a more accurate view of fitness effects.
644 Finally, knockouts were prepared in ancestral backgrounds, ignoring epistatic effects
645 incurred by other mutations accumulated in evolved individuals. We thus acknowledge that
646 our phenotypic data represents an approximation, potentially complemented by more
647 targeted future studies.

648

649 *Future directions*

650 The model of mitonuclear evolution tested in this study predicts that evolutionary
651 divergence is driven by the high rate of evolution experienced by the mitochondrial
652 genome. In turn, the nuclear genome is believed to accumulate compensatory mutations
653 aimed at maintaining compatibility. Data presented in this study support this model by
654 showing the influence of specific mitonuclear interactions on the evolutionary trajectories
655 and range of selected mutations observed in adapting mitonuclear hybrids. We also showed
656 evidence of mitonuclear incompatibility and metabolic disruption in the mitonuclear hybrid
657 ancestors of the experiment. In addition, we provided evidence for the resolution of the
658 incompatibilities. However, this study shows no evidence about the site of compensatory
659 evolution in either the nuclear or mitochondrial genomes. Strains evolved during our
660 experiment may yet enable such demonstrations. Using cytoduction, we may generate
661 novel mitonuclear hybrids by introducing an ancestral mtDNA or nuclear genome into the
662 evolved strains. From a combination of growth, competition and enzymatic assays, along
663 other cellular properties, we should identify which of the nuclear or mitochondrial genome
664 is responsible for compensation. As an example, crossing evolved ND individuals with
665 their ancestor, we could determine if evolved N nuclear genomes converged towards D, or
666 if rather the D mitochondrial genome converged towards N. This experiment would
667 provide an additional test for the standing model of mitonuclear evolution, potentially
668 providing experimental support.

669

670 Our sequencing efforts have identified several mutant loci, with potential relevance to
671 mitochondrial biology and mitonuclear evolution (see **Text S1**). Detailed scrutiny of the
672 cell and molecular biology of adaptive mutations at these loci should provide insight into
673 their underlying mechanisms, shedding light not only on paths of mitonuclear
674 compensation, but also fundamental cellular processes. For example, aneuploidies at
675 chromosome IV have been associated with increased gene dosage at *TSA2* in response to
676 oxidative stress (Linder et al. 2017). We could therefore study the impact of overexpression
677 of this gene in various mitonuclear backgrounds, testing for differential effects. Similarly,
678 artificial expansion of the rDNA locus, as in (Kwan et al. 2016), may help investigate the

679 adaptive influence of chromosome XII copy number on mitonuclear homeostasis. Long
680 read sequencing at *HPF1* and *MNN4* loci in individuals mutant would provide an accurate
681 map of the associated CNVs. This would enable their reconstitution in various
682 backgrounds. Along with already available *RIM20* knockouts, expression of altered *HPF1*
683 and *MNN4* constructs could help to study cell wall mannoproteins. We could further study
684 their role in yeast buoyancy, in addition to their impact on respiration, oxidative stress and
685 chronological lifespan.
686
687 *Summary and conclusion*
688 In this study, we used experimental evolution of yeast mitonuclear hybrids and whole-
689 genome sequencing of the resulting individuals to uncover patterns of evolutionary
690 convergence specific to unique mitonuclear backgrounds. We also confirmed that
691 phenotypic outcomes of evolution are primarily contingent on the nuclear background,
692 with a modulating influence for mitonuclear interactions. We further showed that
693 mitonuclear interactions exert an influence on the molecular mechanisms of adaptation,
694 potentially constraining and potentiating long term evolution. To our knowledge, this study
695 represents the first direct experimental demonstration of mitonuclear interactions inflecting
696 the evolutionary trajectories of adapting populations. In addition to the support provided to
697 standing evolutionary theory, the strains generated in this study and the accumulated data
698 provide material for further studies of mitonuclear evolution and the cell biology of yeast.
699
700 **Materials and Methods**
701
702 **Culture media.** Below are the recipes for the media used in this study. Medium ingredients
703 were purchased from BioShop (Burlington, ON, Canada). Experimental evolution, with its
704 starter cultures, as well as growth and competition assays were all performed in media
705 assembled from ingredients of the same production lot (see below).
706 *Yeast peptone dextrose (YPD)*. 10 g/L yeast extract, 20 g/L tryptone, 20 g/L glucose.
707 2XYPD is assembled by doubling the concentration of all components in YPD.
708 *Yeast peptone glycerol (YPG).* 10 g/L yeast extract, 20 g/L tryptone, 20 g/L glycerol.

709 *Yeast peptone ethanol glycerol (YPEG).* 10 g/L yeast extract, 20 g/L tryptone, 30 g/L
710 ethanol, 20 g/L glycerol.
711 *Enhanced YPD (eYPD).* 15 g/L yeast extract, 40 g/L tryptone, 40 g/L glucose, 5 g/L malt
712 extract, 2.5 g/L glycerol, 0.4 g/L L-cysteine hydrochloride, 0.83 g/L K_2HPO_4, 3 g/L Tris
713 pH 6.0.
714 *Amino acid dropout without uracil and without histidine.* The following compounds were
715 mixed in powder form: 0.5 g L-adenine sulfate dihydrate, 2 g L-arginine hydrochloride, 2
716 g L-aspartic acid, 2 g L-glutamate monosodium salt, 10 g L-leucine, 2 g L-lysine
717 monohydrochloride, 2 g L-methionine, 2 g L-phenylalanine, 2 g L-serine, 2 g L-threonine,
718 2 g L-tryptophan, 2 g L-tyrosine, 2 g L-valine.
719 *Enhanced synthetic complete (eSC).* 3.48 g/L yeast nitrogen base without ammonium
720 sulfate and without amino acids, 2 g/L monosodium glutamate, 40 g/L glucose, 2.5 g/L
721 glycerol, 0.4 g/L L-cysteine hydrochloride, 2.4 g/L amino acid dropout without uracil and
722 without histidine, 0.83 g/L K_2HPO_4, 3 g/L Tris pH 6.0.
723 Solid medium was made by adding 1.5%-2% agar to the above recipes.
724
725 **Screen of collection of yeast cybrids.** A collection of yeast cybrids was previously
726 constituted, as described in (Paliwal et al., 2014; Wolters et al., 2018). It contains all
727 possible combinations of nuclear and mitochondrial genomes from a set of fifteen strains
728 of *S. cerevisiae*, in four biological replicates. Each strain in the collection was assayed for
729 growth in non-fermentable YPG medium as follows. All manipulations were performed
730 following standard sterile technique. Five microliters from thawed glycerol stocks of the
731 collection were transferred to YPD evolution plates and incubated for 48 hours at 30°C,
732 65% relative humidity (RH), with shaking at 165 rpm in a microplate incubator shaker
733 (Multitron, Infors HT, Basel, Switzerland). With the help of a liquid handling robot
734 (Freedom Evo, Tecan, Männedorf, Switzerland), 5 µL from these prolonged cultures were
735 transferred to the wells of a flat bottom polystyrene microtiter plate (Greiner,
736 Kremsmünster, Austria), each well containing 235 µL of YPG and a 2.5 mm diameter glass
737 bead. This second plate was covered with a transparent lid, with sides wrapped in three
738 layers of parafilm (Bemis, Sheboygan Falls, WI, USA). Plate was placed in a Tecan Infinite
739 M Nano microplate reader and incubated for 48 hours at 30°C, recording A_{595} at 20 min

740 intervals. Each 20 min interval consisted of 13 min orbital shaking (6 mm diameter), 5 min
741 absorbance measurement, and 2 min resting time. Raw growth curve data was fitted to a
742 modified Gompertz model, as in (Zwietering et al., 1990). Area under the fitted curve was
743 calculated using the trapezoidal rule.
744
745 **Evolution plates.** Experimental evolution and related experiments were performed in
746 standardized microtiter culture vessels, assembled as follows. Flat-bottom polypropylene
747 microtiter plates, in 96 well format (cat. nb. 951040005, Eppendorf, Hamburg, Germany)
748 served as reusable, autoclavable culture vessels. A clean 2.5 mm diameter glass bead
749 (Biospec, Bartlesville, OK, USA) was placed in each well. Wells were filled with 240 µL
750 media, then sealed with an adhesive foil seal (VWR, Wayne PA, USA). Plates were next
751 covered with clean polypropylene lids held with autoclave tape. Plates were sterilized with
752 a 20 min liquid autoclave cycle at 121°C. Plates were left at room temperature to cool and
753 dry. Plates were then wiped of any residual water, placed in airtight plastic bags, and stored
754 at 4°C until use. Before use, plates were equilibrated at room temperature and centrifuged
755 at 2000 rpm for 2 min. Immediately before inoculation, lids were removed, and foils seals
756 discarded. Following inoculation, plates were sealed with breathable adhesive membranes
757 (VWR, Wayne PA, USA), and covered with polypropylene lids held with masking tape at
758 all four corners. For re-use, plates were emptied, collecting and rinsing beads. Beads were
759 sanitized by a 1 hr+ incubation in warm 10% bleach, rinsed thoroughly with tap water, and
760 dried at 56°C in a Pasteur oven. Plates were washed in soapy water, rinsed thoroughly with
761 tap water, and left inverted at room temperature until fully dry.
762
763 **Assessing the growth of ancestral and evolved individuals on fermentable and non-**
764 **fermentable solid media.** High-throughput assessment of growth in evolved individuals
765 and their ancestral strains was performed by recording the growth of colonies on YPD and
766 YPG agar medium. Replication and array of samples in preparation for growth curves were
767 performed with robotically manipulated pin tools (BM5-SC1, S&P Robotics, Toronto ON,
768 Canada). Thawed glycerol stocks were replicated from 96-well plates to omnitrays (Nunc,
769 Rochester, NY, USA) in 96-array format on YPD agar medium. Replicas were incubated
770 at 30°C until large, well-defined colonies were visible. Replicas were then cherry-picked

771 and re-arrayed to 384-array format on YPD agar, randomizing positions. Following
772 outgrowth, plates were combined into 1,536-array format on YPD agar omnitrays. Evolved
773 individuals of a given mitonuclear background, evolved in both fermentable and non-
774 fermentable conditions, were printed on a single 1,536 array. Each evolved individual was
775 printed as six replicates. Hence, one 1,536 array was prepared per mitonuclear background
776 for a total of seven arrays, whereas nine replicates of each of the ancestral strains were
777 printed onto all seven arrays. To avoid border effects, top and bottom two rows of the arrays
778 were printed with a filler strain, as were the two extreme left and right columns, and these
779 were excluded from analysis. Next, these randomized arrays in 1,536 format were
780 outgrown, then replicated on YPD and YPG agar. The replicas were incubated at 30°C for
781 48 hrs (YPD) or 72 hrs (YPG) in a spImager custom robotic platform (S&P Robotics),
782 recording photographs of the plates at 2-hour intervals. The outgrown replicas were
783 replicated to fresh plates for two additional rounds of growth. Data from the second and
784 third rounds was retained for analysis.
785
786 **Analysis and quantitation of growth on solid medium.** Colony sizes from pictures were
787 measured with R package Gitter (Wagih and Parts, 2014). Growth curves were drawn for
788 each colony, and fitted to a modified Gompertz model, as described above, extracting
789 estimates of the maximum specific growth rate (μ) and carrying capacity (A). Ancestral
790 controls were used to estimate plate-specific effects on growth parameters and to normalize
791 estimates across arrays. Specifically, the effect of a given plate on a growth parameter was
792 calculated by dividing each individual ancestral estimate by the geometric mean of the
793 ancestral estimates over all plates in each carbon source, then extracting the median of that
794 ratio over all ancestral estimates from the same plate. The normalization factor thus
795 obtained was used to multiply all estimates from a plate. True value for growth parameters
796 of any given strain was estimated using the median (if $n \geq 25$) or geometric mean (if $n <$
797 25) over all replicates, with confidence intervals obtained by bootstrapping. A series of
798 two-way ANOVAs with interaction was performed on growth data with nuclear and
799 mitochondrial backgrounds as factors, Separate ANOVAs were conducted for each
800 combination of fitness proxy, evolution regimen, and carbon source.
801

802 **Preparation of whole extracts from strains of *S. cerevisiae* for enzyme assays.**
803 Precultures were inoculated by transferring 5 µL from thawed glycerol stocks to 5 mL
804 2XYPD medium. Cultures were incubated with shaking at 30°C for 24 hrs. Half a milliliter
805 from precultures was used to inoculate 5 mL YPG, and this new culture was incubated with
806 shaking at 30°C for 24 hrs. This second culture was diluted in 45 mL of pre-warmed YPG
807 medium. This subculture was incubated at 30°C with shaking until it reached A_{600}=0.5-1.0.
808 Cells were pelleted by centrifugation, then suspended in water. Cells were pelleted once
809 again by centrifugation, washed in 25 mM potassium phosphate pH 8.0, then frozen as
810 pellets at -80°C. After overnight freezing, pellets were thawed on ice, and suspended in 0.5
811 mL of freshly prepared, ice-cold 25 mM Tris-HCl pH 7.5, 1 mM EDTA, 100 mM NaCl +
812 cOmplete Mini, EDTA-free Protease Inhibitor Cocktail (Roche, Basel, Switzerland).
813 Suspension was bead beaten at 4°C for 10 cycles of 2 min beating, 2 min rest on ice. Lysate
814 was frozen at -80°C.
815
816 **Enzyme assays on whole cell extracts from *S. cerevisiae*.** Enzyme activities were
817 determined spectrophotometrically using a Mithras LB940 microplate reader (Berthold
818 technologies, Germany) and data analyzed with MikroWin 2010 software (Labsis
819 Laborsysteme, Germany). Enzymatic capacities were expressed as mU·mg proteins^{-1}
820 (U·mg proteins^{-1} in the case of CAT), where U refers to 1 µmol of substrate transformed
821 to product per minute. Chemicals were purchased from Sigma-Aldrich (Oakville, Ontario,
822 Canada). Enzymatic assays were performed at 30°C in the following conditions:
823
824 *Malate dehydrogenase (MDH, EC 1.1.1.37)*. MDH activity was measured at 340 nm for 4
825 min, following the oxidation of NADH (ε_{340} = 6.22 mM^{-1}·cm^{-1}). The medium consisted
826 of 100 mM potassium phosphate, 0.2 mM NADH and 0.5 mM oxaloacetate (OAA), pH
827 7.5. The background activity in absence of sample was subtracted from the main results
828 (Bergmeyer, 1983).
829
830 *Mitochondrial complex I + III (ETS, EC 7.1.1.2 and 7.1.1.8).* ETS activity was measured
831 at 490 nm using NADH as electron donor, following the reduction of p-
832 iodonitrotetrazolium violet (INT, ε_{490} = 15.9 mM^{-1}·cm^{-1}) for 6 min. The medium consisted

833 of 50 mM potassium phosphate, 0.85 mM NADH, 2 mM INT and 0.03% (v/v) triton X-
834 100, pH 7.5. The specificity of the reaction was verified in absence of NADH and the
835 residual activity was subtracted from the main results (Hunter-Manseau et al., 2019).
836
837 *Cytochrome c oxidase (CCO, EC 7.1.1.9).* CCO activity was measured at 550 nm following
838 the oxidation of cytochrome c (cyt c, ε_{550} = 18.5 $mM^{-1}\cdot cm^{-1}$) for 6 min. Cyt *c* was reduced
839 through the addition of 4.5 mM dithionite. The medium consisted of 50 mM potassium
840 phosphate, 50 µM cyt c, 1 mM ADP and 0.03% (v/v) triton X-100, pH 7.0. The specificity
841 of the reaction was verified in presence of 40 mM sodium azide (CCO-inhibitor), and the
842 residual activity was subtracted from the main results (Lemaire and Dujardin, 2008;
843 Spinazzi et al., 2012; Hunter-Manseau et al., 2019).
844
845 *ATP-synthase (ATPase, EC 7.1.2.2).* ATPase activity (ATP hydrolysis) was measured at
846 340 nm following the oxidation of NADH (ε_{340} = 6.22 $mM^{-1}\cdot cm^{-1}$) for 4 min. The medium
847 consisted of 250 mM sucrose, 20 mM HEPES, 5 mM $MgSO_4$, 0.35 mM NADH, 2.5 mM
848 phosphoenolpyruvate (PEP), 2.5 mM ATP, 5 µM antimycin A, 4 units · mL^{-1} lactate
849 dehydrogenase (LDH) and 4 units · mL^{-1} pyruvate kinase (PK), pH 8.0. The specificity of
850 the reaction was verified in presence of 25 µM oligomycin (ATPase-inhibitor), and the
851 residual activity was subtracted from the main results (Barrientos et al., 2009; Haraux and
852 Lombes, 2019; Rodriguez et al., 2020).
853
854 *Catalase (CAT, EC 1.11.1.6).* CAT activity was measured at 240 nm following the
855 disappearance of H_2O_2 (ε_{240} = 43.6 $M^{-1}\cdot cm^{-1}$) for 1 min. The medium was composed of
856 100 mM potassium phosphate, 0.1% (v/v) triton X-100 and 60 mM H_2O_2, pH 7.5. The
857 background activity in absence of sample was subtracted from the main results (Page et al.,
858 2009; Pichaud et al., 2010; Orr and Sohal, 1992; Bettinazzi et al., 2021; Christen et al.,
859 2020).
860
861 *Citrate synthase (CS, EC 2.3.3.1).* CS activity was measured at 412 nm for 6 min, following
862 the increase in absorbance due to the reaction between 5,5'-dithiobis-(2-nitrobenzoic acid)
863 (DTNB) and CoA-SH to form TNB (ε_{412} = 14.15 $mM^{-1}\cdot cm^{-1}$). The medium was composed

864 of 100 mM Tris-HCl, 0.1 mM DTNB, 0.1 mM acetyl-CoA (AcCoA), 0.15 mM
865 oxaloacetate (OAA), pH 8.0. The specificity of the reaction was verified in absence of
866 OAA and the residual activity subtracted from the main results (Spinazzi et al. 2012;
867 Hunter-Manseau et al. 2019).
868
869 *Mitochondrial complex II (SDH, EC 1.3.5.1)*. SDH activity was measured at 600 nm using
870 succinate as electron donor and following the reduction of 2,6-dichloroindophenol (DCIP,
871 extinction coefficient ε_{600} = 19.1 $mM^{-1}\cdot cm^{-1}$) for 6 min. To fully activate the enzymatic
872 complex, samples were incubated for 10 min at the assay temperature (30°C) in a reaction
873 medium consisting of 50 mM potassium phosphate, 20 mM succinate and 5 mM $MgCl_2$,
874 pH 7.5. The reaction was started by addition of 50 µM DCIP, 65 µM ubiquinone1 (CoQ1),
875 4 µM antimycin A, 2 µM rotenone and 10 mM sodium azide. The specificity of the reaction
876 was verified in absence of CoQ1 and the residual activity subtracted from the main results
877 (Barrientos et al. 2009; Breton et al. 2009; Spinazzi et al. 2012; Hunter-Manseau et al.
878 2019).
879
880 *Protein content.* Protein concentration ($mg\cdot mL^{-1}$) was determined with the BCA assay
881 (Smith et al., 1985).
882
883 **Preparation of starter cultures for experimental evolution**. All procedures were
884 performed under laminar flow within a sterile enclosure. This protocol was performed
885 identically for strains of each of the following mitonuclear backgrounds: $273614N^{273614N}$
886 (NN), $273614N^{DBVPG6044}$ (ND), $DBVPG6044^{273614N}$ (DN), $DBVPG6044^{DBVPG6044}$ (DD),
887 $DBVPG6044^{Y12}$ (DY), $Y12^{DBVPG6044}$ (YD), $Y12^{Y12}$ (YY). Streaks from each of the four
888 biological replicates from each of the mitonuclear backgrounds were prepared on YPEG
889 agar, and incubated at 30°C for 48 hrs. From each streak, 24 colonies were picked at
890 random with sterile micropipette tips and inoculated into YPD evolution plates. Hence, 96
891 cultures were launched from each of the seven mitonuclear backgrounds submitted to
892 experimental evolution. Plates were incubated overnight at 30°C, 65% RH with shaking at
893 200 rpm. Glycerol stocks were prepared by mixing 100 µL from the starter cultures with
894 100 µL 75% glycerol in the wells of conical bottom polypropylene plates (Greiner,

895 Kremsmünster, Austria). Remainder of the cultures were used immediately to launch
896 experimental evolution.
897
898 **Experimental evolution on mitonuclear hybrids of *S. cerevisiae*.** Our collection of yeast
899 cybrids contains four biological replicates of each mitonuclear background, each derived
900 from a separate cybridization event. Twenty-four evolutions were founded from each of
901 these cybrids, hence 96 replicate populations of each of seven mitonuclear backgrounds
902 were propagated by daily serial passage in both fermentable (YPD) and non-fermentable
903 (YPG) medium for 58 days. All procedures were performed under laminar flow within a
904 sterile enclosure. Starter cultures were used to inoculate a first batch of experimental
905 evolution cultures. With the help of a liquid handling robot (Freedom Evo 150, Tecan,
906 Männedorf, Switzerland), 5 µL from each starter culture were transferred to YPD evolution
907 plates, and in parallel to YPG evolution plates. Tips used for transfer were washed with
908 sterile water and kept for further transfer of the same cultures. Plates were incubated for 24
909 hrs at 30°C, 65% RH with shaking at 200 rpm. Evolving populations were then transferred
910 to new evolution plates for 58 consecutive days. On day 2 and every 7 days afterwards
911 until day 58, glycerol stocks were prepared by mixing 100 µL from the evolving
912 populations with 100 µL 75% glycerol in the wells of conical bottom polypropylene plates.
913
914 **Isolation of independently evolved individuals.** Glycerol stocks from day 58 of the
915 evolution experiment were thawed at room temperature. Ten microliters from each stock
916 were transferred to the surface of a YPD agar petri dish. The resulting drop from the
917 glycerol stock was streaked for single colonies. Petri dishes were incubated for 48 hrs at
918 30°C. From each Petri dish, a single colony was picked at random using a sterile tip and
919 placed into a YPG evolution plate. Plates were incubated for 24 hrs at 30°C, 65% RH with
920 shaking at 200 rpm. Glycerol stocks were prepared by mixing 100 µL from the starter
921 cultures with 100 µL 75% glycerol in the wells of conical bottom polypropylene plates
922 (Greiner, Kremsmünster, Austria).
923
924 **Preparation of total DNA from evolved individuals and ancestral strains.** Total DNA
925 from each individual evolved strain and all ancestral strains was extracted and purified as

926 starting material for the preparation of next-generation sequencing libraries. A custom
927 protocol using the DNeasy Blood and Tissue Kit (Qiagen, Venlo, Netherlands) was applied
928 in 96-well format. Each strain was inoculated from glycerol stock in 4 x 1 mL YPD
929 medium, in a polypropylene 96-well deep well plate (DWP). Each DWP was covered with
930 a breathable adhesive membrane and incubated for 24 hours at 30°C with shaking at 200
931 rpm. Cells were harvested by centrifugation for 10 min at 5000 x g and suspended in 250
932 µL water. Suspensions of each strain were pooled into a single well, and centrifuged once
933 more for 10 min at 5000 x g. Pellets were suspended in 600 µL of 1 M sorbitol, 100 mM
934 sodium EDTA, 14 mM β-mercaptoethanol, supplemented with 6 U zymolyase (Bioshop,
935 Burlington ON, Canada), then transferred to collection microtubes provided with the
936 DNeasy kit, and incubated at 30°C for at least 30 min. Resulting spheroplasts were pelleted
937 by centrifugation for 10 min at 5000 x g, suspended in 180 µl Buffer ATL + 20 µl proteinase
938 K solution, and mixed thoroughly. Lysis suspensions were incubated at 56°C for at least
939 30 min, mixing occasionally to disperse the samples. Samples were shaken vigorously for
940 15 s, then centrifuged briefly to collect all liquid at the bottom of tubes. Samples were
941 supplemented with 4 µL of 100 mg/mL RNase A, mixed vigorously, and incubated at room
942 temperature for at least 5 min. A 50:50 mix of buffer AL and ethanol was prepared fresh,
943 and 400 µL were dispensed to each tube, mixing once again by vortexing. Lysates (max
944 900 µL) were applied to DNeasy 96 purification columns. Columns were centrifuged for
945 10 min at 3800 x g. Columns were washed with 500 µL buffer AW1, centrifuging for 5
946 min at 3800 x g. Columns were further washed with 500 µL buffer AW2, centrifuging for
947 15 min at 3800 x g. Columns were next placed on a clean rack of elution microtubes and
948 100 µL of buffer AE were added to each sample. Samples were incubated for at least 1 min
949 at room temperature, then centrifuged for 2 min at 3800 x g. Each eluate was next
950 supplemented with 4 µL of 10 mg/mL RNase A, agitated vigorously, and incubated at room
951 temperature for 15 min. The RNase-treated eluates were further purified by mixing 50 µL
952 from each sample with 20 µL beads and incubating at room temperature for 5 min. After
953 the bead mixture was applied to a magnet for 60s, liquid was removed from the beads,
954 which were washed twice with 200 µL of 80% ethanol. Beads were suspended in 40 µL of
955 10 mM Tris-HCl pH 8.0 and incubated for 5 min at room temperature. Eluate was separated
956 from beads using a magnet, as described above. Sample quality was evaluated by agarose

957 gel electrophoresis. Purity and concentration of DNA was assessed by measuring
958 absorbance at 260 nm and 280 nm using a NanoDrop spectrophotometer (ThermoFisher
959 Scientific, Waltham MA, USA). Concentration of DNA in the sample was further
960 estimated using the AccuClear Ultra High Sensitivity dsDNA Quantitation Kit (Biotium,
961 Fremont CA, USA) following manufacturer's instructions.
962
963 **Preparation of next-generation sequencing libraries.** Sequencing libraries were
964 prepared using the Tagment DNA Enzyme and Buffer Large Kit (Illumina, San Diego CA,
965 USA), the KAPA HiFi HotStart ReadyMix 2X (Roche, Basel, Switzerland) and custom
966 DNA barcodes. Genomic DNA samples were diluted with water to a target concentration
967 of 2.5 ng/µL or less. Tagmentation reactions were assembled by mixing 1.25 µL tagment
968 DNA buffer, 0.25 µL tagment DNA enzyme and 1 µL gDNA dilution. Reactions were
969 incubated at 55°C for 5 min. Custom DNA barcodes were added by PCR as follows.
970 Tagmented DNA was mixed with 3.76 µL 2X KAPA ReadyMix, and 0.625 µL both
971 primers. Primers had sequences 5'AATGATACGGCGACCACCGAGATCTACAC-(8-
972 nucleotide custom i5 barcode)-TCGTCGGCAGCGTC3' and
973 5'CAAGCAGAAGACGGCATACGAGAT-(8-nucleotide custom i7 barcode)-
974 GTCTCGTGGGCTCGG3'. A collection of 32 custom i5 barcodes and 48 custom i7
975 barcodes was used, enabling the preparation of 1,536 unique barcode combinations. PCR
976 was performed by cycling as follows: 72°C for 3 min, 98°C for 2:45 min, then 8 cycles of
977 98°C for 15s, 62°C for 30s, 72°C for 3 min, followed by a 1 min final extension at 72°C.
978 Library preparation was completed by reconditioning PCR. Barcoding reactions were
979 mixed with 8.5 µL 2X KAPA ReadyMix, 0.5 µL of 10 µM primer P1
980 (5'AATGATACGGCGACCACCGA3') and 0.5 µL of 10 µM primer P2
981 (5'CAAGCAGAAGACGGCATACGA3'). Reactions were then cycled as follows: 95°C
982 for 5 min, then 4 cycles of 98°C for 20s, 62°C for 20s, 72°C for 2 min, followed by a 2 min
983 final extension at 72°C. Final PCR products were diluted with 14 µL PCR grade water,
984 then bead purified as described above, except that only 18 µL beads were added to the PCR
985 reactions. Library concentration was estimated using the AccuClear Ultra High Sensitivity
986 dsDNA Quantitation Kit following manufacturer's instructions. A subset of the libraries
987 was inspected with a BioAnalyzer 2100 using a High Sensitivity DNA chip (Agilent

988 Technologies, Santa Clara CA, USA) for insert size and monodispersity. Equimolar
989 amounts of all libraries were pooled and sequenced on an Illumina NovaSeq6000 S4 PE150
990 sequencing lane at the Génome Québec Expertise and Service Center (Montréal QC,
991 Canada).
992
993 **Pre-treatment of sequencing results and alignment to reference genomes**. Quality
994 control was performed individually on each sequencing library using FastQC (Andrews,
995 2010), and results were aggregated using MultiQC (Ewels et al., 2016). Sequencing
996 adapters were trimmed with Trimmomatic (Bolger et al., 2014). Overlapping read pairs
997 were merged using BBmerge (Bushnell et al., 2017). Single read files from the BBmerge
998 output were concatenated into single files. Primary read mapping to reference genomes
999 was performed using bwa mem (Li and Durbin, 2009). Libraries were mapped to the
1000 published genomes of their associated ancestral strains. The *S. cerevisiae* 273614N
1001 reference genome sequence was obtained from the diArk database (Hammesfahr et al.,
1002 2011) as published in (Liti et al., 2009). Reference genome sequences for *S. cerevisiae*
1003 strains DBVPG6044 and Y12 were obtained from NCBI BioProject PRJEB7245,
1004 BioSamples SAMEA2757762 and SAMEA2757763, respectively, as published in (Yue et
1005 al., 2017). Chimeric reference genomes were assembled for cybrid strains by manually
1006 replacing the mitochondrial genome contig published for the nuclear parent's genome with
1007 that published for the mitochondrial parent. Alignment was performed separately for
1008 merged and paired reads. Hence, BAM outputs from bwa mem were merged and then
1009 sorted with samtools (Li et al., 2009). Following the addition of read groups and
1010 deduplication with picard (Broad Institute, 2016), indel realignment was performed using
1011 GATK3 (McKenna et al., 2010; van der Auwera and O'Connor, 2020). Alignment and
1012 depth metrics were collected using picard and samtools, respectively. Whole-genome
1013 pileups were extracted for each sequencing library with samtools.
1014
1015 **Estimating the fraction of mtDNA per cell.** The fraction of sequence bases mapped to
1016 coding regions of the mitochondrial genome was used as a proxy for copy number,
1017 structural or other changes incurred to the organellar genome. This was computed from
1018 pileup, summing the depth of coverage with base quality greater than 20 in known coding

1019 regions of the reference mitochondrial genomes. This sum across the mitochondrial
1020 genome divided by the same sum over the whole genome provided an estimate of the
1021 fraction of coding mitochondrial DNA in each cell.
1022
1023 **Identification of aneuploidies from sequencing data.** Aneuploidies were called from
1024 pileup. Telomeric and subtelomeric regions were excluded from this analysis by masking
1025 25 kb at both ends of each chromosome. High quality depth of coverage was computed at
1026 each position by counting reads with both base and mapping quality above 30 on the phred
1027 scale. Finally, any position found with average depth of coverage in all biological replicates
1028 of the ancestral strains above 5 times the median depth over the whole genome was also
1029 excluded from analysis. Next, the ratio between the mean depth of the chromosome and
1030 that of the rest of the genome was calculated. If this ratio was between 0.75 and 1.25, a p-
1031 value for the mean coverage of the chromosome was computed, assuming normal
1032 distribution of depth of coverage across the genome, with mean and standard deviation
1033 computed over the rest of the genome. If this p-value was smaller than the length of the
1034 chromosome divided by the length of the whole genome, an aneuploidy was suspected.
1035 Aneuploidy candidates were confirmed visually by inspecting heatmaps of depth of
1036 coverage along the length of chromosomes.
1037
1038 **Primary identification of copy number variants (CNVs) from sequencing data.**
1039 Primary CNV calling was performed essentially according to (Yoon et al., 2009). Analysis
1040 was performed from filtered pileups, as described above for aneuploidies. Each
1041 chromosome was divided in 100 bp windows, extracting mean depth of coverage for each
1042 window. Average and standard deviation on window means were computed across
1043 chromosomes, enabling computation of a z-score and p-value for each window. Next,
1044 whole chromosomes were scanned with rolling intervals of various window sizes, starting
1045 with 2 windows in length. If the maximum p-value for windows within an interval fell
1046 below a threshold, determined by both window and chromosome length, the interval was
1047 marked as a candidate CNV. Increasing interval sizes were used until a threshold
1048 determined by both interval and chromosome length was reached. Overlapping CNV
1049 candidates were merged. Any candidate with median depth between 0.75x and 1.25x the

1050 median chromosome depth was excluded. A p-value was computed for the mean depth of
1051 each candidate, based on mean and standard deviation over windows. If this p-value was
1052 greater than 10^{-6}, the candidate was excluded. Finally, if the same area had mean depth of
1053 coverage between 0.75x and 1.25x the chromosome-wide median depth in the ancestral
1054 strains, the candidate CNV was also excluded.
1055
1056 **Resolution of artefactual CNV calls caused by misalignment at homologous loci.**
1057 Reference genome sequence at CNV coordinates were blasted against the whole reference
1058 genome sequence, identifying loci with high homology to CNV candidates. Blast hits with
1059 an E-value of less than 1.0, length above 150 bp and percent identity with the CNV locus
1060 above 80% were retained for further scrutiny. Sequences at the CNV call and homologous
1061 hit loci were aligned with MUSCLE (Edgar, 2004), identifying locus specific positions. A
1062 system of linear equations was built from the sums of each base calls at each locus specific
1063 positions in the alignment. Multiple linear regression was then used to identify the most
1064 likely depth of coverage, with 95% confidence interval, at each homologous locus. If the
1065 inferred depth was between 0.75x and 1.25x the chromosome median depth, and the
1066 confidence interval on depth at the homologous locus did not overlap with the confidence
1067 interval for depth over the whole chromosome, a CNV call was asserted. Otherwise, or if
1068 locus specific information was too scarce to lift ambiguity caused by homology, CNV call
1069 was not retained. Applying this methodology, several CNVs were rejected, others were
1070 retained, while a subgroup was reassigned to more likely loci.
1071
1072 **SNV calling.** Primary SNV calling was performed using two parallel methods, starting
1073 with GATK HaplotypeCaller. SNV calls were combined into a single GVCF file using
1074 GATK CombineGVCF. Initial filtering was performed with GATK FilterVariants and
1075 SelectVariants. Additional filtering was done with vcftools. A list of SNVs was produced
1076 in csv format using bcftools.
1077
1078 In parallel, custom SNV calling was attempted directly from pileup. The following regions
1079 of the genome were filtered out of pileups in preparation for SNV calling: high coverage
1080 regions in the ancestral strains, subtelomeric regions, positions with mean base and

1081 mapping quality below 30, positions with depth of coverage below 10, and positions with
1082 N or otherwise missing sequence in the reference. A baseline error model was built,
1083 identifying the number of each base call expected at each position, considering the
1084 reference base and mean base quality at that position, and the average error rates observed
1085 in the data. A chi^2 test for goodness of fit was performed, comparing the expected base
1086 counts predicted by the error model with the observed base counts. An E-value was
1087 obtained by multiplying this p-value with the number of positions in the genome. Positions
1088 with an E-value < 1.0 were retained as potential SNVs, while any position with non-
1089 reference base call count less than 25% of total depth was rejected.
1090
1091 The intersection between the results of both primary SNV calling pipelines was kept as the
1092 overall primary list of SNVs. SNV calls were additionally filtered for strand, base quality
1093 and mapping quality biases. A few libraries were observed to display SNVs that overlapped
1094 strongly with those from libraries that were found in close proximity on library preparation
1095 plates. Those SNVs were flagged as potential cross-contamination artifacts and removed
1096 from further scrutiny. Furthermore, SNVs found in two or more libraries that shared a
1097 barcode were tagged as potential index hopping artifacts and removed from SNV calls.
1098 Moreover, the same substitutions arising repeatedly at the exact same position were
1099 deemed unlikely: any SNV encountered in four libraries or more was rejected. SNVs
1100 expected to arise from alignment of reads to the wrong reference genome (e.g.
1101 DBVPG6044 reads mistakenly aligned to the Y12 reference genome) were also removed.
1102 Next, using Fisher's exact test, SNV calls were identified that were more compatible with
1103 the homozygous non-mutant genotype than the heterozygous or homozygous mutant
1104 scenarios, and thus rejected. Finally, libraries that presented an unusually high number of
1105 SNVs (more than 300 SNVs and more than 2 standard deviations above average number
1106 of SNVs per library) were rejected. A heterozygous genotype was called for many SNVs,
1107 despite uniformly haploid starting populations. A small sample of evolved individuals were
1108 thus assessed for ploidy, as described above, showing diploidization in approximately half
1109 sampled isolates (**Fig S15**).
1110

1111 **Annotation of CNV and SNV calls.** Annotations of the S288c reference genome (Engel
1112 et al., 2022) were used for annotating SNV and CNV calls in evolved isolates. Sequences
1113 from mutation-carrying loci were blasted against the S288c reference genome to identify
1114 corresponding coordinates. Annotations corresponding to these locations were identified
1115 with Yeastmine (Balakrishnan et al., 2012).
1116
1117 **Analysis of dissimilarity between mutational profiles.** Mutational profiles were built for
1118 each combination of mitonuclear background and evolution regimen (evolutionary
1119 circumstances) by counting mutations associated with each mutant annotation. Bray-Curtis
1120 dissimilarity was computed between the mutational profiles of all pairs of evolutionary
1121 circumstances. Non-parametric multi-dimensional scaling was performed from the
1122 resulting dissimilarity matrix, preserving the best from 10 000 independent initializations
1123 of the algorithm. The algorithm was run for a maximum of 3000 iterations, declaring
1124 convergence using a stress tolerance threshold of 10^{-9}.
1125
1126 **Specificity of mutant loci for carbon sources and nuclear and mitochondrial**
1127 **backgrounds.** The same strategy was applied to test the specificity of mutant loci for
1128 carbon source, nuclear background, mitochondrial background, and all combinations
1129 thereof. For each locus, a contingency table was assembled reporting counts of mutations
1130 within and outside the locus in each category. This table was submitted to a chi^2 test of
1131 independence, yielding a p-value. Mutual information (MI, reported as dits) was calculated
1132 from the same contingency table. Significance thresholds on chi^2 p-values were corrected
1133 for false discovery rate on all loci. Loci with chi^2 p-value below threshold and mutual
1134 information two standard deviations above mean MI were deemed non-randomly
1135 distributed between categories, and thus displaying specificity.
1136
1137 **Analysis of association between phenotypic changes and mutant loci.** Quantitative
1138 phenotypic data, including fitness proxies (carrying capacity and growth rate) in both
1139 fermentable and non-fermentable media, as well as the fraction of mtDNA per cell, are
1140 available for each evolved mutant. A list of annotated mutations is also associated with
1141 each mutant, enabling tests of the statistical association between mutant loci and

1142 phenotypic changes. For each mutant locus and each phenotype in each carbon source, the
1143 association was tested as follows. A t-test was performed to determine if the fitness of
1144 individuals that display mutations at the locus of interest differed significantly from fitness
1145 of their ancestral strains, yielding a p-value. In parallel, using the same data, effect size of
1146 mutation at the locus was evaluated by calculating Cohen's *d* corrected for sample size,
1147 with associated standard error. P-value of obtaining a given effect size at least as extreme
1148 by chance was computed empirically by drawing 10 000 random samples of the same size
1149 among mutants of the same mitonuclear background and calculating an effect size for each.
1150 These calculations were performed separately for each mitonuclear background since
1151 ancestral strains displayed widely differing phenotypes. P-values obtained for each
1152 mitonuclear background were combined using Stouffer's method, with the square root of
1153 sample sizes used as weights. Significance thresholds were corrected for false discovery
1154 rate applying the method of Benjamini and Hochberg on all loci as described in (Kuo,
1155 2017). Loci with both p-values below threshold were deemed significantly associated with
1156 quantitative changes in phenotype.
1157
1158 **Generation of fluorescent knock-out mutants at putative loss-of-function loci.** First,
1159 GFP- and mCherry-tagged derivatives of all ancestral strains were generated from three
1160 biological replicates. Parental strains all carried the *MATa ho::hphMX ura3::KanMX*
1161 genotype. They were transformed with both the GFP and mCherry selection cassettes,
1162 which shared the same general structure. The expression of both fluorescent proteins was
1163 placed under the control of the *S. cerevisiae TEF2* promoter and *ENO1* terminator.
1164 Fluorescent protein expression cassettes were fused to the *natNT2* selection cassette. This
1165 full-length cassette was flanked on both extremities with 40 bp homology to the *HIS3* locus
1166 and transformed into the ancestral strains using the lithium acetate method. Transformants
1167 were selected on eYPD agar medium (as described in *Culture media* subsection above)
1168 supplemented with 100 µg/mL hygromycin, 100 µg/mL geneticin and 75 µg/mL
1169 nourseothricin. Integration of the fluorescent protein expression cassettes at the *HIS3* locus
1170 was confirmed by growth in presence of nourseothricin, loss of histidine prototrophy,
1171 detection of a fluorescent signal by flow cytometry and successful PCR amplification at
1172 the 5' and 3' junctions between the *HIS3* locus and heterologous sequences. Knockouts of

1173 each of the following genes were prepared in all fluorescent derivatives of the ancestral
1174 strains: *AMN1*, *GPB2*, *IRA2*, *MNN4*, *RIM20*, *SIR3*, *SIR4*, and *SUC2*. Open reading frames
1175 at each of these loci were deleted by transformation with the *Kluyveromyces lactis URA3*
1176 expression cassettes amplified from plasmid pUG72 (Gueldener et al., 2002) and flanked
1177 in 5' and 3' with 40 bp homology to the promoters and terminators of the target genes.
1178 Transformants were selected on eSC agar devoid of uracil. Knockouts were scored for
1179 uracil prototrophy; resistance to hygromycin, geneticin and nourseothricin; detection of a
1180 fluorescent signal by flow cytometry and successful PCR amplification at the 5' and 3'
1181 junctions between the target locus and heterologous deletion cassette.
1182
1183 **Competition assays between knockouts and their ancestral strains.** Changes in fitness
1184 incurred by deletion at loci of interest were quantified by performing competition assays
1185 in fermentable and non-fermentable media, using a method inspired by (Breslow et al.,
1186 2008). Knockouts at each of the eight loci of interest, in the mitonuclear background under
1187 study, as three biological replicates, labeled with both GFP and mCherry were arrayed as
1188 glycerol stocks in 96-well format. Matching arrays of the fluorescently labeled ancestors
1189 were also prepared. Precultures in 96-well format of both the ancestral and knock-out
1190 strains were inoculated by transferring 5 μL from thawed glycerol stock arrays to YPD
1191 evolution plates. These preculture plates were incubated for 24 hrs at 30°C, 65% RH with
1192 shaking at 200 rpm. Outgrown precultures of the knockouts and matching ancestral strains
1193 were mixed by transferring 5 μL from both to YPD and YPG evolution plates. Control
1194 competitions of the mCherry and GFP labeled ancestral strains were also prepared, to
1195 account for differences in fitness caused by the fluorescent labels. For three consecutive
1196 days following mixing of the strains, competition cultures were propagated and transferred
1197 as described above for experimental evolution. On each day, outgrown cultures were
1198 diluted 1:50 in non-sterile water. Two thousand cells from each dilution were analyzed by
1199 flow cytometry, counting mCherry and GFP positive cells. Flow cytometry measurements
1200 were performed with the help of a Guava easyCyte HT (Luminex, Austin TX, USA) or
1201 Accuri C6 (BD, Franklin Lakes NJ, USA) instrument. All microbiological procedures were
1202 performed under laminar flow within a sterile enclosure, except for endpoint measurement
1203 by flow cytometry. All pipetting was performed with the help of a liquid handling robot

1204 (Freedom Evo, Tecan, Männedorf, Switzerland). Triplicate competitions were performed
1205 on both fluorescent derivatives of all biological replicates in both carbon sources.
1206
1207 **Analysis of competition data.** The $\log_2$ ratio of mCherry count over GFP count was
1208 calculated for each time point in each competing culture. The $\log_2$ ratio at time zero was
1209 subtracted from time points of a given competition so that samples may share a common
1210 y-intercept. Linear regression was performed on all data points derived from the same
1211 biological replicate, fitting to the following model:
1212
1213 $$log_2 \frac{n_{mCherry}}{n_{GFP}} = \Delta\mu_{WTvWT}\mathrm{t} + \Delta\mu_{KO}\mathrm{tM} + \beta_0$$
1214
1215 where $n_{mCherry}$ is the number of mCherry-labeled cells, n_{GFP} is the number of GFP-labeled
1216 cells, $\Delta\mu_{WTvWT}$ is the difference in growth rate between the mCherry and GFP labeled
1217 ancestor, t is time, $\Delta\mu_{KO}$ is the difference in growth rate between the knock-out and its
1218 ancestor, M is a variable with value 0 when a time point belongs to a ancestor vs ancestor
1219 competition, and 1 when it belongs to a knock-out vs ancestor competition, and β_0 is a
1220 constant. The fit thus provides an estimate for the change in growth rate associated with
1221 knocking out the gene of interest in the current mitonuclear background. Standard error
1222 (SE) on this coefficient estimate is used to test whether the coefficient is null, and to
1223 compute a sum-of-squares error (SS) on the estimate. Estimates for three biological
1224 replicates and two fluorescent labels thus provided six estimates for each locus in each
1225 mitonuclear background. They were combined into a single estimate by calculating an
1226 average weighted by sample size. P-values were combined using Stouffer's method,
1227 weighted by sample size. Similarly, sum-of-square errors were combined by summing
1228 them and adding the product of sample size with the square deviation of each estimate
1229 from the overall mean estimate. Mean fitness effect estimates, and the combined sum-of-
1230 squares were used to perform ANOVAs to test if fitness effect of a given locus in each
1231 carbon source differed between mitochondrial backgrounds, with accompanying Tukey
1232 HSD tests on pairwise differences between backgrounds. Similarly, ANOVAs were
1233 performed to determine if fitness effects of loci differed on given mitonuclear
1234 backgrounds. Two-way ANOVAs were performed to determine significance of nuclear,

1235 mitochondrial, and mitonuclear interaction effects on growth rate changes. Spearman
1236 rank correlation was calculated between fitness effects estimated by competition assays
1237 and frequency of mutations at the loci in each background, as determined from
1238 sequencing data.
1239
1240 **Mutational bias.** We counted every possible single nucleotide change among all SNV
1241 calls in our dataset, and assigned them to their corresponding mitonuclear background.
1242 Counts of for each mitonuclear background were compared to the dataset-wide counts
1243 applying a chi^2-test of independence, with a p-value threshold of 0.05.
1244
1245 **Assessment of ploidy in select strains.** Ploidy was determined for all ancestral strains and
1246 a subset among evolved individuals, following a method inspired by (Charron et al. 2019).
1247 Thawed glycerol stocks of the strains were streaked for single colonies on YPD agar. Single
1248 colonies were picked in triplicate and inoculated into 1 mL YPD, in wells of a
1249 polypropylene DWP. DWPs were incubated for 24 hrs at room temperature. Cells were
1250 washed with 2 x 1 mL water, then fixed for 1 hr in 70% ethanol. Ethanol was removed by
1251 washing cells twice with 1 mL water. Cells were next incubated overnight at 37°C in 1 mL
1252 of freshly prepared 0.25 mg/mL RNase A. Cells were washed twice with 1 mL of 50 mM
1253 sodium citrate pH 7.0. A small volume (25 µL) of the washed cell suspension was diluted
1254 in 225 µL of 0.667 µM SYTOX green (Thermo Fisher Scientific) and incubated in the dark
1255 at room temperature for 1 hr. Cell density in the stained sample was adjusted to
1256 approximately 500 cells/µL, and analyzed by flow cytometry, recording 5000 events per
1257 sample. Mean green fluorescence was measured for cells in G1 phase. All manipulations
1258 were performed in triplicate.
1259
1260 **Acknowledgements**
1261
1262 This work was supported by the Natural Science and Engineering Research Council of
1263 Canada (Discovery grant to CRL, RGPIN-2020-04844), the Fonds de recherche du
1264 Québec – Nature et Technologies (Team grant 2019-PR-254415 to CRL and SBr) and the
1265 Canada Research Chair in Cellular Systems and Synthetic Biology to CRL. DBP was

supported by an award from the Fonds de recherche du Québec – Santé (FRQS). During part of the writing/reviewing, SBe was supported by the European Union's Horizon 2020 research and innovation programme under the Marie Skłodowska-Curie grant agreement No 101030803. Raw sequencing data is available on the NCBI sequence read archive under BioProject accession number PRJNA878596.

Authors contributions

Conceptualization: CRL, DBP, HLF, SBr

Data curation: DBP

Investigation: AKD, CB, DBP, SBe

Methodology: AKD, CRL, DBP, HLF, IGA, SBe, SBr,

Resources: CRL, HLF, SBr

Software: DBP

Supervision: CRL, HLF, SBr

Validation: AKD, DBP

Visualization: DBP

Writing – original draft preparation: DBP

Writing – review and editing: all authors

Formal analysis: DBP, SBe

Project administration: CRL

Funding acquisition: CRL and SBr

References

Allen JF, Horner DS, Cavalier-Smith T, Willison K, Leaver CJ, Martin W. 2003. The function of genomes in bioenergetic organelles. In: Philosophical Transactions of the Royal Society B: Biological Sciences.

Barreto FS, Watson ET, Lima TG, Willett CS, Edmands S, Li W, Burton RS. 2018. Genomic signatures of mitonuclear coevolution across populations of Tigriopus californicus. *Nat Ecol Evol* 2:1250–1257.

Barrientos A, Fontanesi F, Díaz F. 2009. Evaluation of the Mitochondrial Respiratory Chain and Oxidative Phosphorylation System Using Polarography and Spectrophotometric Enzyme Assays. *Curr Protoc Hum Genet* 63.

Barrientos A, Kenyon L, Moraes CT. 1998. Human Xenomitochondrial Cybrids. *Journal of Biological Chemistry* 273:14210–14217.

1300 Bendich AJ. 1996. Structural Analysis of Mitochondrial DNA Molecules from
1301 Fungi and Plants Using Moving Pictures and Pulsed-field Gel Electrophoresis.
1302 Bendich AJ. 2007. The size and form of chromosomes are constant in the nucleus,
1303 but highly variable in bacteria, mitochondria and chloroplasts. *BioEssays*
1304 29:474–483.
1305 Bernardi G. 2005. Lessons from a small, dispensable genome: The mitochondrial
1306 genome of yeast. *Gene* 354:189–200.
1307 Blount ZD, Borland CZ, Lenski RE. 2008. Historical contingency and the evolution
1308 of a key innovation in an experimental population of Escherichia coli. *Proc*
1309 *Natl Acad Sci U S A* 105:7899–7906.
1310 Breslow DK, Cameron DM, Collins SR, Schuldiner M, Stewart-Ornstein J, Newman
1311 HW, Braun S, Madhani HD, Krogan NJ, Weissman JS. 2008. A comprehensive
1312 strategy enabling high-resolution functional analysis of the yeast genome. *Nat*
1313 *Methods* 5:711–718.
1314 Breton S, Beaupré HD, Stewart DT, Piontkivska H, Karmakar M, Bogan AE, Blier
1315 PU, Hoeh WR. 2009. Comparative mitochondrial genomics of freshwater
1316 mussels (Bivalvia: Unionoida) with doubly uniparental inheritance of mtDNA:
1317 Gender-specific open reading frames and putative origins of replication.
1318 *Genetics* 183:1575–1589.
1319 Bull JJ, Molineux IJ. 2008. Predicting evolution from genomics: experimental
1320 evolution of bacteriophage T7. *Heredity (Edinb)* [Internet] 100:453–463.
1321 Available from: www.nature.com/hdy
1322 Burton RS. 2022. The role of mitonuclear incompatibilities in allopatric speciation.
1323 *Cellular and Molecular Life Sciences* 79:103.
1324 Burton RS, Barreto FS. 2012. A disproportionate role for mtDNA in Dobzhansky-
1325 Muller incompatibilities? *Mol Ecol* 21:4942–4957.
1326 Caudal E, Friedrich A, Jallet A, Garin M, Hou J, Schacherer J. 2022. Loss-of-
1327 function mutation survey revealed that genes with background-dependent
1328 fitness are rare and functionally related in yeast. Available from:
1329 https://doi.org/10.1073/pnas.2204206119
1330 Charron G, Marsit S, Hénault M, Martin H, Landry CR. 2019. Spontaneous whole-
1331 genome duplication restores fertility in interspecific hybrids. *Nat Commun* 10.
1332 Chen P, Michel AH, Zhang J. 2022. Transposon insertional mutagenesis of diverse
1333 yeast strains suggests coordinated gene essentiality polymorphisms. *Nat*
1334 *Commun* 13.
1335 Chou HH, Chiu HC, Delaney NF, Segrè D, Marx CJ. 2011. Diminishing returns
1336 epistasis among beneficial mutations decelerates adaptation. *Science (1979)*
1337 332:1190–1192.
1338 Chou JY, Hung YS, Lin KH, Lee HY, Leu JY. 2010. Multiple molecular
1339 mechanisms cause reproductive isolation between three yeast species. *PLoS*
1340 *Biol*.
1341 Cooper CE, Nicholls P, Freedman JA. 1991. Cytochrome c oxidase: structure,
1342 function, and membrane topology of the polypeptide subunits. *Biochemistry*
1343 *and Cell Biology* 69:586–607.

1344 Cooper TF, Rozen DE, Lenski RE. 2003. Parallel changes in gene expression after
1345 20 , 000 generations of evolution in Escherichia coli. *Proc Natl Acad Sci U S A*
1346 100:1072–1077.
1347 Couce A, Tenaillon OA. 2015. The rule of declining adaptability in microbial
1348 evolution experiments. *Front Genet* 6.
1349 Desai N, Brown A, Amunts A, Ramakrishnan V. 2017. The structure of the yeast
1350 mitochondrial ribosome. *Science (1979)* 355:528–531.
1351 Dey R, Barrientos A, Moraes CT. 2000a. Functional constraints of nuclear
1352 mitochondrial DNA interactions in xenomitochondrial rodent cell lines.
1353 *Journal of Biological Chemistry*.
1354 Dey R, Barrientos A, Moraes CT. 2000b. Functional Constraints of Nuclear-
1355 Mitochondrial DNA Interactions in Xenomitochondrial Rodent Cell Lines.
1356 *Journal of Biological Chemistry* 275:31520–31527.
1357 Dowling DK. 2014. Mitonuclear interactions: evolutionary consequences over
1358 multiple biological scales. *Philos Trans R Soc Lond B Biol Sci*.
1359 Dyall SD, Brown MT, Johnson PJ. 2004. Ancient Invasions: From Endosymbionts
1360 to Organelles. *Science (1979)*.
1361 Ferreira GC. 1995. Heme biosynthesis: Biochemistry, molecular biology, and
1362 relationship to disease. *J Bioenerg Biomembr* 27:147–150.
1363 Freel KC, Friedrich A, Schacherer J. 2015. Mitochondrial genome evolution in
1364 yeasts: An all-encompassing view. *FEMS Yeast Res*.
1365 Fritsch E, Chabbert C, Klaus B, Steinmetz L. 2014. A Genome-Wide Map of
1366 Mitochondrial DNA Recombination in Yeast. *Genetics* 198:755–771.
1367 Fritsch ES, Chabbert CD, Klaus B, Steinmetz LM. 2014. A genome-wide map of
1368 mitochondrial DNA recombination in yeast. *Genetics*.
1369 Galeota-Sprung B, Fernandez A, Sniegowski P. 2022. Changes to the mtDNA copy
1370 number during yeast culture growth. *R Soc Open Sci* [Internet] 9. Available
1371 from: https://royalsocietypublishing.org/doi/10.1098/rsos.211842
1372 Gueldener U, Heinisch J, Koehler GJ, Voss D, Hegemann JH. 2002. A second set of
1373 loxP marker cassettes for Cre-mediated multiple gene knockouts in budding
1374 yeast. *Nucleic Acids Res* [Internet] 30:e23. Available from:
1375 http://www.pubmedcentral.nih.gov/articlerender.fcgi?artid=101367&tool=pmc
1376 entrez&rendertype=abstract
1377 Haddad R, Meter B, Ross JA. 2018. The Genetic Architecture of Intra-Species
1378 Hybrid Mito-Nuclear Epistasis. *Front Genet* 9:1–11.
1379 Hagström E, Freyer C, Battersby BJ, Stewart JB, Larsson NG. 2014. No
1380 recombination of mtDNA after heteroplasmy for 50 generations in the mouse
1381 maternal germline. *Nucleic Acids Res*.
1382 Havird JC, Sloan DB. 2016. The roles of mutation, selection, and expression in
1383 determining relative rates of evolution in mitochondrial versus nuclear
1384 genomes. *Mol Biol Evol*.
1385 Hendrich L, Pons J, Ribera I, Balke M. 2010. Mitochondrial Cox1 Sequence Data
1386 Reliably Uncover Patterns of Insect Diversity But Suffer from High Lineage-
1387 Idiosyncratic Error Rates. *PLoS One*.
1388 Herron MD, Doebeli M. 2013. Parallel Evolutionary Dynamics of Adaptive
1389 Diversification in Escherichia coli. *PLoS Biol* 11.

1390 Hill GE. 2015. Mitonuclear ecology. *Mol Biol Evol*.
1391 Hunte C, Palsdottir H, Trumpower BL. 2003. Protonmotive pathways and
1392 mechanisms in the cytochrome bc1 complex. *FEBS Lett* 545:39–46.
1393 Hunter-Manseau F, Desrosiers V, le François NR, Dufresne F, Detrich HW, Nozais
1394 C, Blier PU. 2019. From Africa to Antarctica: Exploring the Metabolism of
1395 Fish Heart Mitochondria Across a Wide Thermal Range. *Front Physiol* 10.
1396 Jordá T, Puig S. 2020. Regulation of Ergosterol Biosynthesis in Saccharomyces
1397 cerevisiae. *Genes (Basel)* 11:795.
1398 Kenyon L, Moraes CT. 2002. Expanding the functional human mitochondrial DNA
1399 database by the establishment of primate xenomitochondrial cybrids.
1400 *Proceedings of the National Academy of Sciences*.
1401 Kim DU, Hayles J, Kim D, Wood V, Park HO, Won M, Yoo HS, Duhig T, Nam M,
1402 Palmer G, et al. 2010. Analysis of a genome-wide set of gene deletions in the
1403 fission yeast Schizosaccharomyces pombe. *Nat Biotechnol* 28:617–623.
1404 Kvitek DJ, Sherlock G. 2013. Whole Genome, Whole Population Sequencing
1405 Reveals That Loss of Signaling Networks Is the Major Adaptive Strategy in a
1406 Constant Environment. *PLoS Genet* 9.
1407 Kwan EX, Wang XS, Amemiya HM, Brewer BJ, Raghuraman MK. 2016. rDNA
1408 Copy Number Variants Are Frequent Passenger Mutations in Saccharomyces
1409 cerevisiae Deletion Collections and de Novo Transformants. *G3*
1410 *Genes|Genomes|Genetics* 6:2829–2838.
1411 Lane N. 2011. Mitonuclear match: Optimizing fitness and fertility over generations
1412 drives ageing within generations. *BioEssays*.
1413 Lane N, Martin W. 2010. The energetics of genome complexity. *Nature*.
1414 Lang GI, Botstein D, Desai MM. 2011. Genetic Variation and the Fate of Beneficial
1415 Mutations in Asexual Populations. *Genetics* 188:647–661.
1416 Lang GI, Rice DP, Hickman MJ, Sodergren E, Weinstock GM, Botstein D, Desai
1417 MM. 2013. Pervasive genetic hitchhiking and clonal interference in forty
1418 evolving yeast populations. *Nature* 500:571–574.
1419 Lee HY, Chou JY, Cheong L, Chang NH, Yang SY, Leu JY. 2008. Incompatibility
1420 of Nuclear and Mitochondrial Genomes Causes Hybrid Sterility between Two
1421 Yeast Species. *Cell*.
1422 Lenski RE. 2017. Experimental evolution and the dynamics of adaptation and
1423 genome evolution in microbial populations. *Nature Publishing Group* [Internet]
1424 11:2181–2194. Available from: www.nature.com/ismej
1425 Linder RA, Greco JP, Seidl F, Matsui T, Ehrenreich IM. 2017. The Stress-Inducible
1426 Peroxidase TSA2 Underlies a Conditionally Beneficial Chromosomal
1427 Duplication in Saccharomyces cerevisiae. *G3 Genes|Genomes|Genetics*
1428 7:3177–3184.
1429 Łuksza M, Lässig M. 2014. A predictive fitness model for influenza. *Nature* 507.
1430 Lynch M, Koskella B, Schaack S. 2006. Mutation pressure and the evolution of
1431 organelle genomic architecture. *Science (1979)*.
1432 Lynch M, Sung W, Morris K, Coffey N, Landry CR, Dopman EB, Dickinson WJ,
1433 Okamoto K, Kulkarni S, Hartl DL, et al. 2008. A genome-wide view of the
1434 spectrum of spontaneous mutations in yeast. *Proceedings of the National*
1435 *Academy of Sciences* 105:9272–9277.

1436 Ma H, Marti Gutierrez N, Morey R, van Dyken C, Kang E, Hayama T, Lee Y, Li Y,
1437 Tippner-Hedges R, Wolf DP, et al. 2016. Incompatibility between Nuclear and
1438 Mitochondrial Genomes Contributes to an Interspecies Reproductive Barrier.
1439 *Cell Metab* [Internet] 24:283–294. Available from:
1440 http://dx.doi.org/10.1016/j.cmet.2016.06.012
1441 Malina C, Larsson C, Nielsen J. 2018. Yeast mitochondria: an overview of
1442 mitochondrial biology and the potential of mitochondrial systems biology.
1443 *FEMS Yeast Res* 18.
1444 Mangin M, Faugeron-Fonty G, Bernardi G. 1983. The orir to ori+ mutation in
1445 spontaneous yeast petites is accompanied by a drastic change in mitochondrial
1446 genome replication. *Gene* 24:73–81.
1447 Mason PA, Lightowlers RN. 2003. Why do mammalian mitochondria possess a
1448 mismatch repair activity? *FEBS Lett*.
1449 Mcdonald MJ. 2019. Microbial Experimental Evolution-a proving ground for
1450 evolutionary theory and a tool for discovery. *EMBO Rep* 20.
1451 Mcdonald MJ, Gehrig SM, Meintjes PL, Zhang X-X, Rainey PB. 2009. Adaptive
1452 Divergence in Experimental Populations of Pseudomonas fluorescens. IV.
1453 Genetic Constraints Guide Evolutionary Trajectories in a Parallel Adaptive
1454 Radiation. *Genetics* [Internet] 183:1041–1053. Available from:
1455 www.genetics.org/
1456 McKenzie M, Trounce I. 2000. Expression of Rattus norvegicus mtDNA in Mus
1457 musculus cells results in multiple respiratory chain defects. *Journal of*
1458 *Biological Chemistry*.
1459 Meyer JR, Dobias DT, Weitz JS, Barrick JE, Quick RT, Lenski RE. 2012.
1460 Repeatability and Contingency in the Evolution of a Key Innovation in Phage
1461 Lambda. *Science (1979)* 335:428–432.
1462 Nguyen THM, Sondhi S, Ziesel A, Paliwal S, Fiumera HL. 2020. Mitochondrial-
1463 nuclear coadaptation revealed through mtDNA replacements in Saccharomyces
1464 cerevisiae. *BMC Evol Biol* 20.
1465 Niki Y, Chigusa SI, Matsuura ET. 1989. Complete replacement of mitochondrial
1466 DNA in Drosophila. *Nature*.
1467 Osuský M, Kissová J, Kováč L. 1997. Interspecies transplacement of mitochondria
1468 in yeasts. *Curr Genet*.
1469 Paliwal S, Fiumera AC, Fiumera HL. 2014. Mitochondrial-nuclear epistasis
1470 contributes to phenotypic variation and coadaptation in natural isolates of
1471 saccharomyces cerevisiae. *Genetics*.
1472 Puddu F, Herzog M, Selivanova A, Wang S, Zhu J, Klein-Lavi S, Gordon M,
1473 Meirman R, Millan-Zambrano G, Ayestaran I, et al. 2019. Genome architecture
1474 and stability in the Saccharomyces cerevisiae knockout collection. *Nature*
1475 573:416–420.
1476 Read AD, Bentley RET, Archer SL, Dunham-Snary KJ. 2021. Mitochondrial iron–
1477 sulfur clusters: Structure, function, and an emerging role in vascular biology.
1478 *Redox Biol* 47:102164.
1479 Robba L, Russell SJ, Barker GL, Brodie J. 2006. Assessing the use of the
1480 mitochondrial cox1 marker for use in DNA barcoding of red algae
1481 (Rhodophyta). *Am J Bot*.

1482 Rutter J, Hughes AL. 2015. Power2: The power of yeast genetics applied to the
1483 powerhouse of the cell. *Trends in Endocrinology & Metabolism* 26:59–68.
1484 Spinazzi M, Casarin A, Pertegato V, Salviati L, Angelini C. 2012. Assessment of
1485 mitochondrial respiratory chain enzymatic activities on tissues and cultured
1486 cells. *Nat Protoc* 7:1235–1246.
1487 Špírek M, Horváth A, Piškur J, Sulo P. 2000. Functional co-operation between the
1488 nuclei of Saccharomyces cerevisiae and mitochondria from other yeast species.
1489 *Curr Genet*.
1490 Spirek M, Polakova S, Jatzova K, Sulo P. 2015. Post-zygotic sterility and
1491 cytonuclear compatibility limits in S. cerevisiae xenomitochondrial cybrids.
1492 *Front Genet* 5.
1493 Tenaillon O, Rodriguez-Verdugo A, Gaut RL, McDonald P, Bennett AF, Long AD,
1494 Gaut BS. 2012. The Molecular Diversity of Adaptive Convergence. *Science*
1495 335:457–461.
1496 Vijayraghavan S, Kozmin SG, Strope PK, Skelly DA, Lin Z, Kennell J, Magwene PM,
1497 Dietrich FS, McCusker JH. 2019. Mitochondrial Genome Variation Affects Multiple
1498 Respiration and Nonrespiration Phenotypes in Saccharomyces cerevisiae. *Genetics*
1499 211:773–786.
1500 Weinreich DM, Delaney NF, DePristo MA, Hartl DL. 2006. Darwinian Evolution
1501 Can Follow Only Very Few Mutational Paths to Fitter Proteins. *Science (1979)*
1502 [Internet] 312:111–114. Available from:
1503 http://www.sciencemag.org/content/312/5770/111.abstract\nhttp://www.science
1504 mag.org/content/312/5770/111.full.pdf
1505 Wichman HA, Badgett MR, Scott LA, Boulianne CM, Bull JJ. 1999. Different
1506 Trajectories of Parallel Evolution During Viral Adaptation. *Science (1979)*
1507 285:422–424.
1508 Wiser M, Ribeck N, Lenski R. 2013. Long-term dynamics of adaptation in asexual
1509 populations. *Science (1979)* 342:1364–1367.
1510 Wolters JF, Charron G, Gaspary A, Landry CR, Fiumera AC, Fiumera HL. 2018.
1511 Mitochondrial recombination reveals mito–mito epistasis in yeast. *Genetics*
1512 209:307–319.
1513 Wolters JF, Chiu K, Fiumera HL. 2015. Population structure of mitochondrial
1514 genomes in Saccharomyces cerevisiae. *BMC Genomics* [Internet] 16:1–13.
1515 Available from: http://dx.doi.org/10.1186/s12864-015-1664-4
1516 Xu F, Addis JBL, Cameron JM, Robinson BH. 2012. LRPPRC mutation suppresses
1517 cytochrome oxidase activity by altering mitochondrial RNA transcript stability
1518 in a mouse model. *Biochemical Journal* 441:275–283.
1519 Yamaoka M, Isobe K, Shitara H, Yonekawa H, Miyabayashi S, Hayashi JI. 2000.
1520 Complete repopulation of mouse mitochondrial DNA-less cells with rat
1521 mitochondrial DNA restores mitochondrial translation but not mitochondrial
1522 respiratory function. *Genetics*.
1523 Zakharov I, Yarovoy B. 1977. Cytoduction as a new tool in studying cytoplasmic
1524 heredity in yeast. *Mol Cell Biochem* 14:15–18.
1525 de Zamaroczy M, Marotta R, Faugeron-Fonty G, Coursot R, Mangin M, Baldacci G,
1526 Bernardi G. 1981. The origins of replication of the yeast mitochondrial genome
1527 and the phenomenon of suppressivity. *Nature* 292:75–78.

1528

1529

1530 **Figure 1.** Adaptive evolution of mitonuclear hybrids. **(A)** *Yeast strains submitted to*
1531 *experimental evolution were derived from strains 273614N (NN), DBVPG6044 (DD) and*
1532 *Y12 (YY). Cytoduction of NN and YY with DD yielded two cybrids each. (ND and DN, DY*
1533 *and YD). We thus evolved seven ancestral mitonuclear backgrounds.* **(B)** *Each of these*
1534 *backgrounds was evolved in fermentable (FF) and non-fermentable (NF) media, as 96*
1535 *replicates. Evolving populations were propagated for approximately 300 generations by*
1536 *daily robot-assisted serial passage. At the end of the experiment, a single independently*
1537 *evolved individual was isolated from each population. Evolved individuals were assessed*
1538 *for growth rate in fermentable* **(C)** *and non-fermentable* **(D)** *media, showing significant*
1539 *gains in fitness in most cases. Asterisks indicate median fitness in evolved strains*
1540 *significantly higher than ancestors (Mann-Whitney U-test p-value < 0.05).*
1541
1542 **Figure 2.** Whole-genome sequencing reveals mitonuclear background- and carbon
1543 source-specific genomic changes in experimental evolution isolates. **(A)** *Fraction of*
1544 *sequenced bases mapped to the mitochondrial genome was used as a proxy for the*
1545 *proportion of DNA belonging to the mitochondrial genome, revealing a mitonuclear*
1546 *background-specific impact for both cytoduction and evolution.* **(B)** *Changes in*
1547 *chromosome copy numbers (aneuploidies), and smaller, gene-scale copy number variants*
1548 *(CNVs) we detected using depth of coverage information. Many single-nucleotide*
1549 *variants (SNVs) were also called. All those changes were unevenly distributed among*
1550 *mitonuclear backgrounds and carbon sources.*
1551
1552 **Figure 3.** Mutation at certain loci is associated with quantitative phenotype changes.
1553 *Mutant loci associated with quantitative changes in phenotype were identified by*
1554 *performing two statistical tests. Scatter plots show on the x-axis the negative log p-value*
1555 *that individual mutants at a given locus have phenotype identical to their parents, and on*
1556 *the y-axis, the negative log p-value that a phenotypic effect of this size could be observed*
1557 *from a set of random individuals of equal size. Dotted lines indicate significance*
1558 *thresholds for p-values > 0.05, corrected for false-discovery rate. Color of the data*
1559 *points indicates the mitonuclear background most often affected by mutation at the locus,*
1560 *while shape indicates carbon source in which the locus was most often mutant. This*
1561 *analysis was performed for carrying capacity* **(A, B)** *and growth rate* **(C, D)***, in*
1562 *fermentable* **(A, C)** *and non-fermentable* **(B, D)** *media, as well as for the fraction of*
1563 *mtDNA per cell* **(E).**
1564

1565 **Figure 4.** Mutations display convergence that is carbon source and mitonuclear specific.
1566 *Loci were considered specific for a certain carbon source* ***(A)*** *or mitonuclear background*
1567 ***(B)*** *if their distribution among categories differed significantly from that of all detected*
1568 *mutations, taken as a whole. Chi^2 tests were performed on contingency tables of all*
1569 *mutations, classifying them as mapping or not to the locus, and according to either*
1570 *carbon source or mitonuclear background. Mutual information was calculated from the*
1571 *same contingency tables. Specificity thresholds, indicated by dotted lines, were set at a p-*
1572 *value of 0.05, corrected for false-discovery rate, and at two standard deviations above*
1573 *mean (~95th percentile) mutual information across all loci.*
1574

Figure 5. Fitness effect for loss-of-function at select loci is dependent on mitonuclear background and carbon source. *Gene knockouts were performed at the indicated loci in fluorescent-derivatives of all seven ancestral strains used in the evolution experiment, mimicking loss-of-function alleles. These knockouts were competed against their deletion-free counterparts of the same mitonuclear genotype in fermentable (***top***) and non-fermentable (***bottom***) media. This enabled estimation of the fitness effect of loss-of-function at these loci, reported in shades of red (positive effect) or blue (negative effect). For each locus, effect of deletion was found to differ significantly between mitonuclear genotypes (ANOVA p-value < 0.01). Similarly, loci had differing effects on any given mitonuclear genotype (ANOVA p-value < 0.01). Fitness effect of each locus in across mitonuclear genotypes did not correlate with frequency of mutation at the locus in each genotype, with one exception indicated by an asterisk on the right-hand side (spearman rho > 0.95). Asterisks at the top of heatmaps indicate genotypes that display rank order correlation between locus fitness effect preference and frequency of mutation at the locus (spearman rho > 0.7, p-value<0.05 that slope of regression =0).*

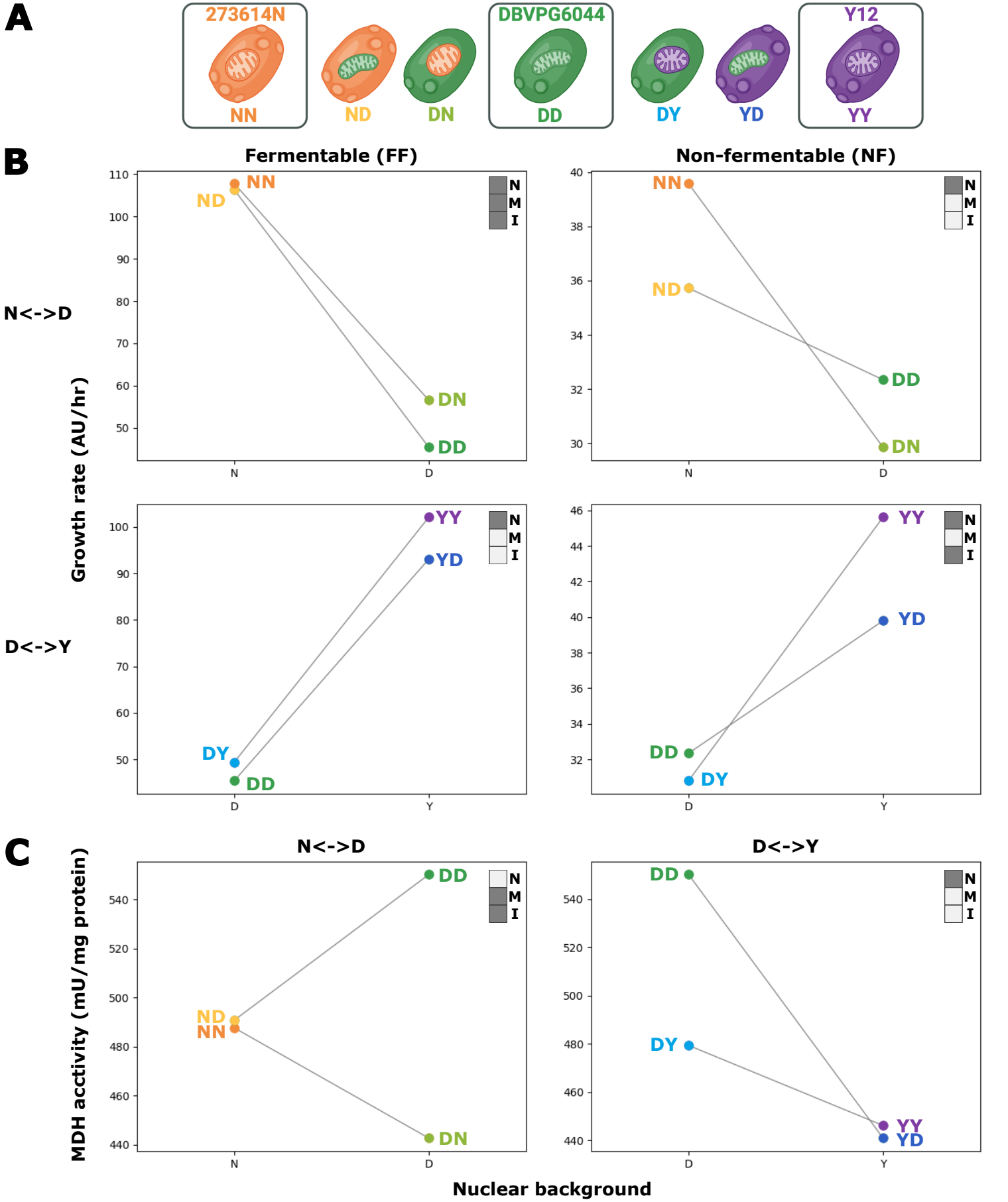
A
273614N
NN
ND
DN
DBVPG6044
DD
DY
YD
Y12
YY
B
Fermentable (FF)
Non-fermentable (NF)
N<->D
D<->Y
Growth rate (AU/hr)
N
M
I
C
N<->D
D<->Y
MDH acctivity (mU/mg protein)
Nuclear background

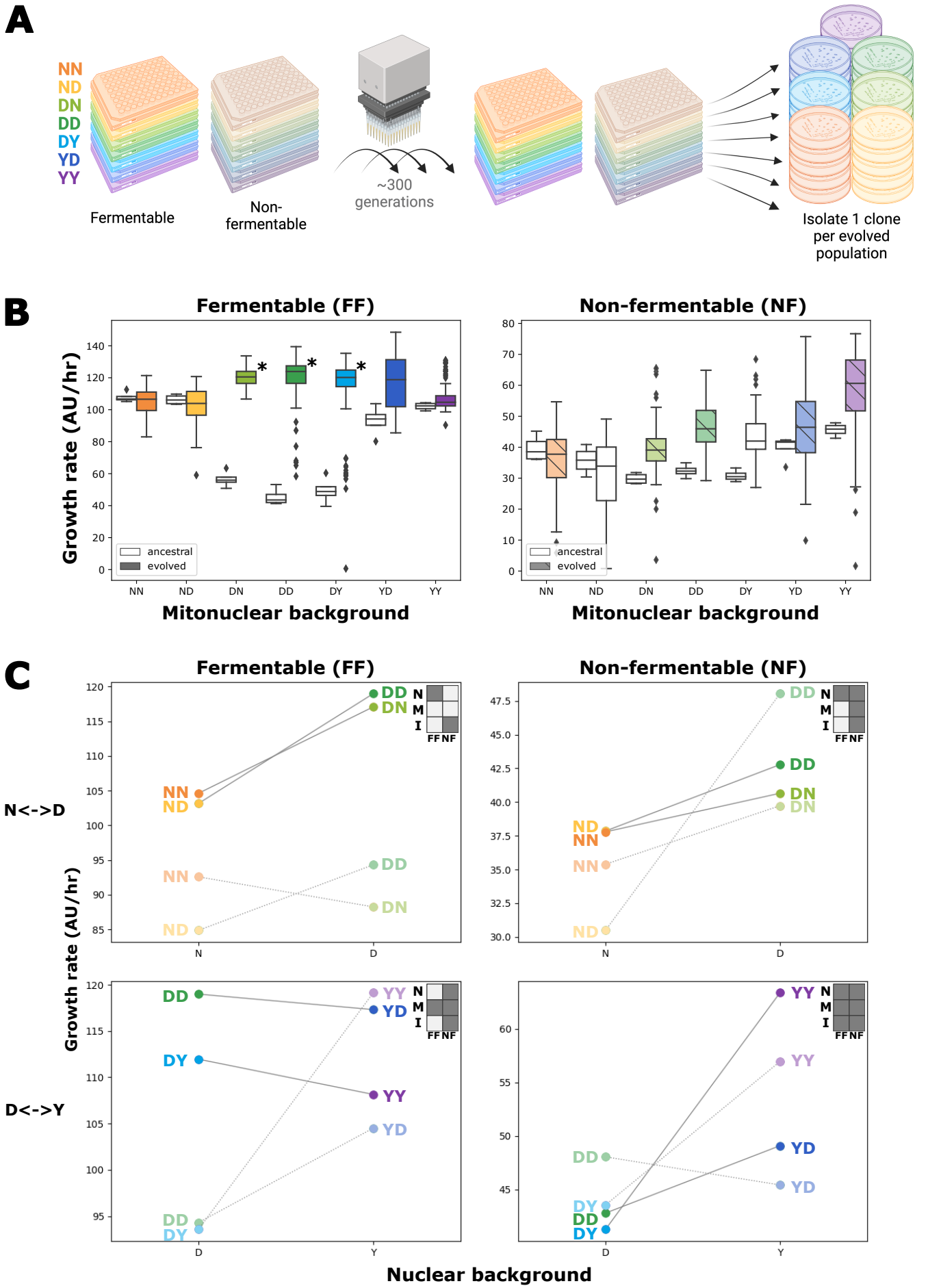
A
NN
ND
DN
DD
DY
YD
YY
Fermentable
Non-fermentable
~300 generations
Isolate 1 clone per evolved population
B
Fermentable (FF)
Non-fermentable (NF)
Growth rate (AU/hr)
ancestral
evolved
NN ND DN DD DY YD YY
Mitonuclear background
C
Fermentable (FF)
Non-fermentable (NF)
N<->D
D<->Y
Growth rate (AU/hr)
N M I
FF NF
Nuclear background

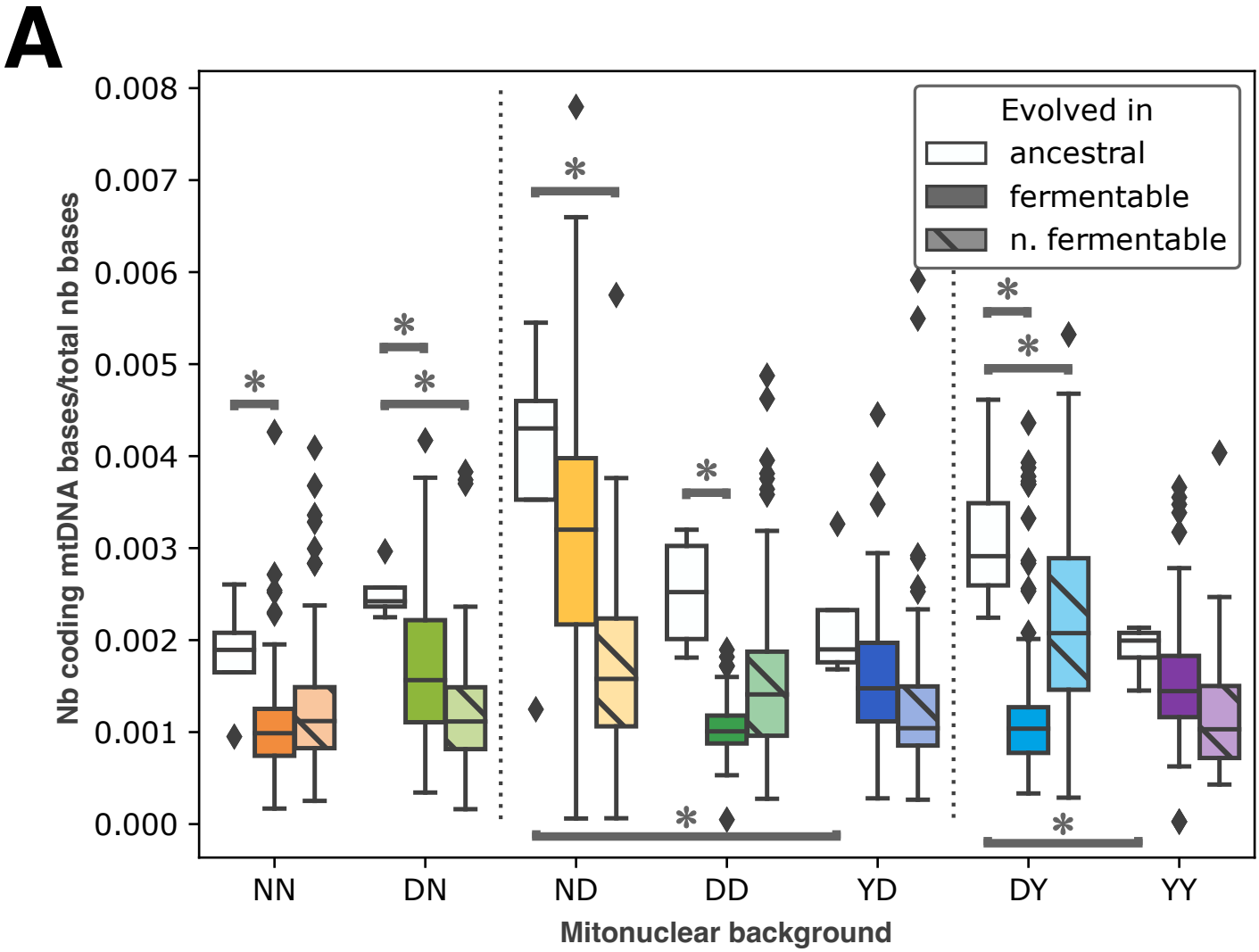
A
Evolved in
ancestral
fermentable
n. fermentable
Nb coding mtDNA bases/total nb bases
0.008
0.007
0.006
0.005
0.004
0.003
0.002
0.001
0.000
NN
DN
ND
DD
YD
DY
YY
Mitonuclear background

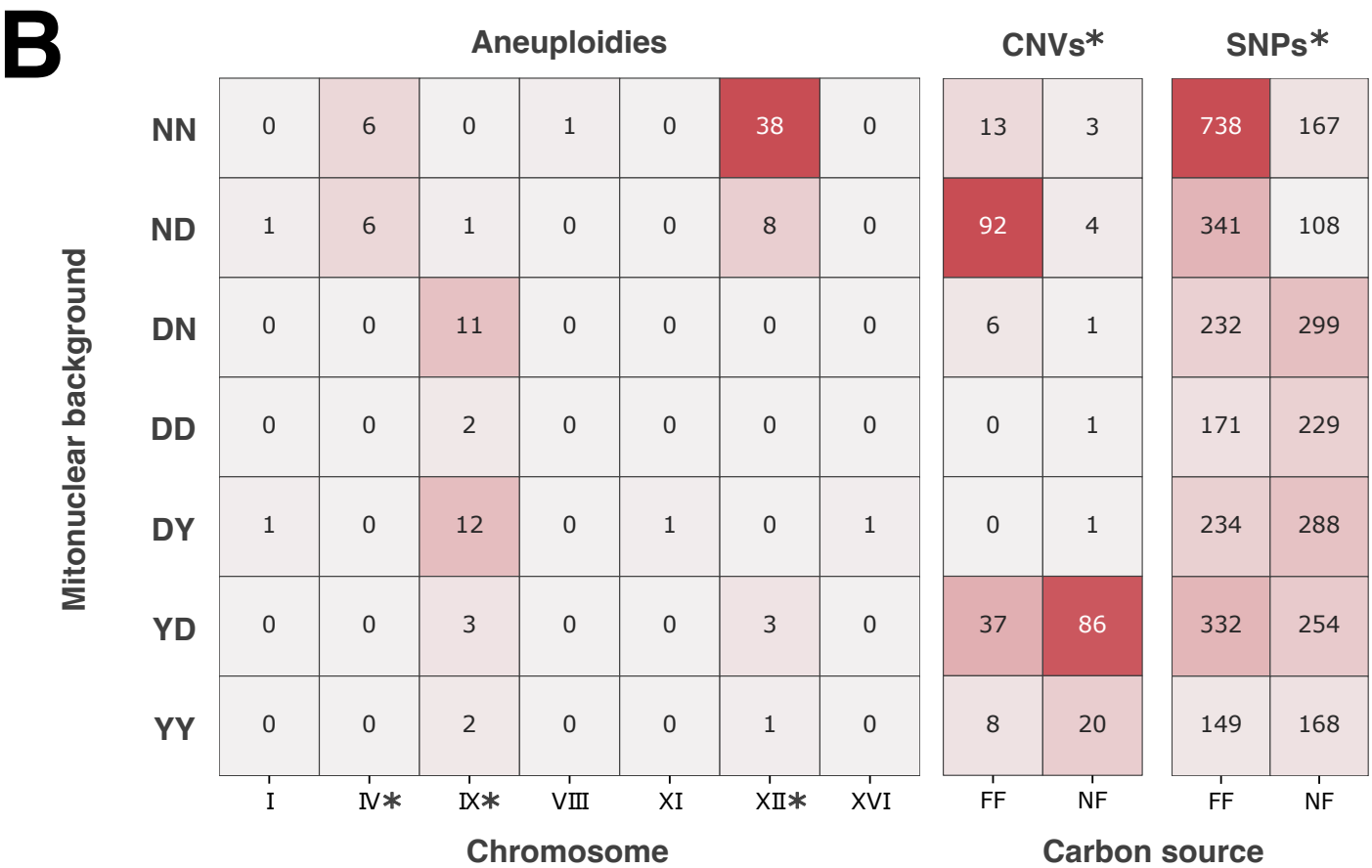
B
Aneuploidies
CNVs*
SNPs*
Mitonuclear background
NN 0 6 0 1 0 38 0 13 3 738 167
ND 1 6 1 0 0 8 0 92 4 341 108
DN 0 0 11 0 0 0 0 6 1 232 299
DD 0 0 2 0 0 0 0 0 1 171 229
DY 1 0 12 0 1 0 1 0 1 234 288
YD 0 0 3 0 0 3 0 37 86 332 254
YY 0 0 2 0 0 1 0 8 20 149 168
I
IV*
IX*
VIII
XI
XII*
XVI
FF
NF
FF
NF
Chromosome
Carbon source

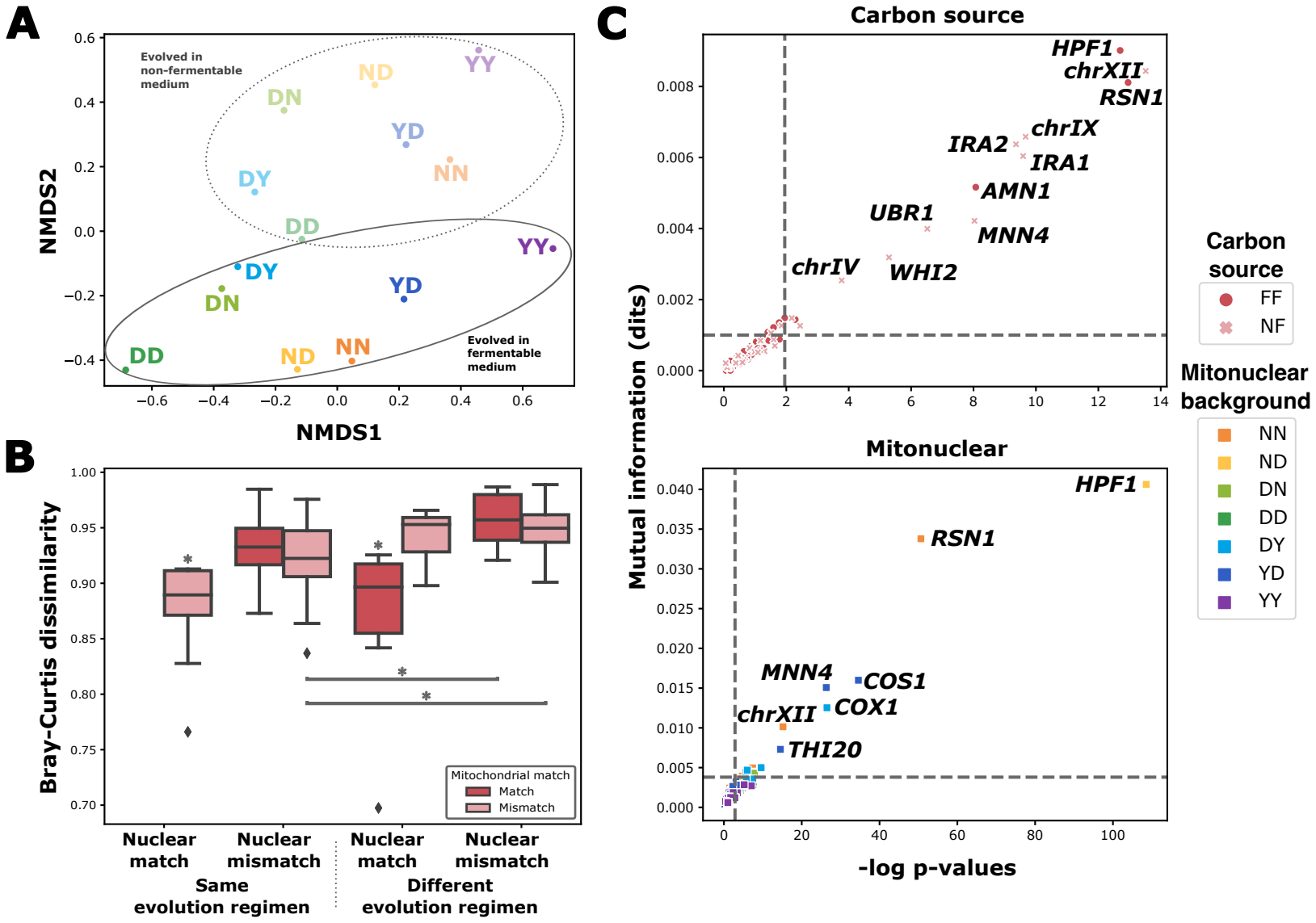
A
Evolved in non-fermentable medium
Evolved in fermentable medium
NMDS1
NMDS2
B
Bray-Curtis dissimilarity
Mitochondrial match
Match
Mismatch
Nuclear match
Nuclear mismatch
Nuclear match
Nuclear mismatch
Same evolution regimen
Different evolution regimen
C
Carbon source
Mitonuclear
Mutual information (dits)
-log p-values
HPF1
chrXII
RSN1
chrIX
IRA2
IRA1
AMN1
UBR1
MNN4
chrIV
WHI2
COS1
COX1
THI20
Carbon source
FF
NF
Mitonuclear background
NN
ND
DN
DD
DY
YD
YY

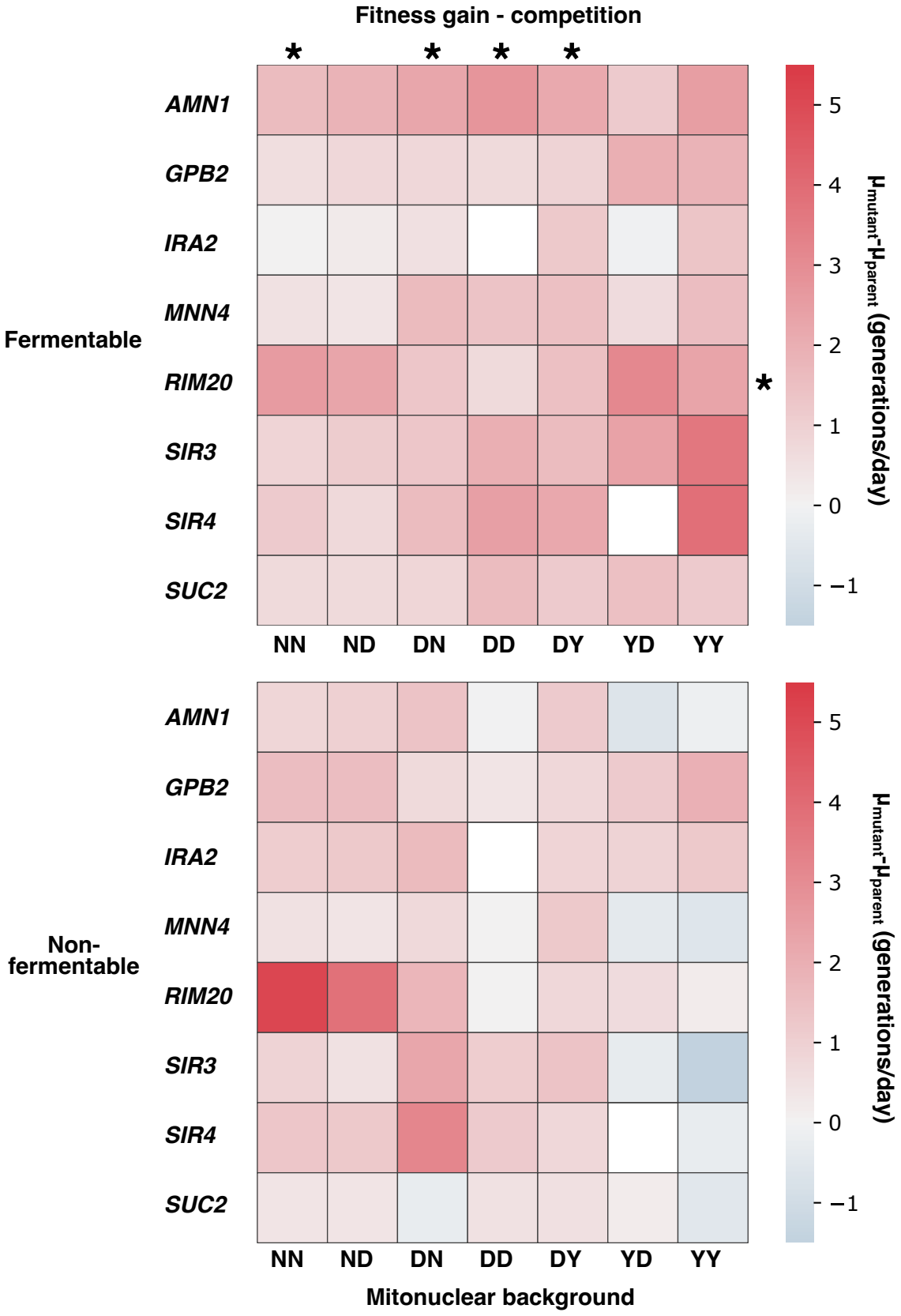
Fitness gain - competition
*
*
*
*
AMN1
GPB2
IRA2
MNN4
RIM20
SIR3
SIR4
SUC2
Fermentable
*
NN
ND
DN
DD
DY
YD
YY
5
4
3
2
1
0
−1
μmutant-μparent (generations/day)
Non-fermentable
Mitonuclear background